# Influenza pandemic risk factors associated with solar cycle extremes, low solar and geomagnetic activity, cold-glacial climate change and geographic origination (1500-2018).

Author information

Carlton B. Brown[1]¶ *

**1** Affiliations: Veterinarian, private researcher and author, Taumarunui, New Zealand.

*Corresponding author

Email: carlton@grandsolarminimum.com (CBB)

## Abstract

There is no means of predicting when influenza pandemics could occur because risk factors are poorly understood. Risk factor assessment utilized numerous statistical methods, 10 multi-century solar activity and climate change datasets, and expert reviewed influenza outbreaks. The mid-study coldest temperature was compared with glacial cycle peak temperatures (n=16 ice cores). There was a grand mean 0.92 pandemics per 11-year sunspot number cycle (SE=0.15, n=25, 1700-) and a higher pandemic probability at cycle peaks and troughs +/-1-year (logistic regression, Peaks: P=0.01, OR=4.2. Troughs: P=0.03, OR=3.4). Multiple logistic regression confirmed peak+trough+/-1-year stages and positive cosmic ray intensity anomalies relative to its 1961-1990 mean as pandemic and epidemic predictors-triggers respectively (Pr>|z|<0.05, 1700-). Simple logistic1 and linear2 regression identified colder Greenland and Northern Hemisphere temperatures, increased cosmic ray intensity, Arctic sea ice cover, and Greenland ice accumulation rate relative to their 1961-1990 means as outbreak1 and annual outbreak rate2 predictors (P<0.05, 1-11yr moving average1 and cycle mean2 anomalies, 1500-1, 1700-1,2). Greenland was at its coldest mid-study, 8-kiloyears after the glacial cycle peak temperature (mean -4.8°C, n=10 ice cores), or -21% of its prior Holocene interglacial increase. Four categories of risk factors were identified, including

solar cycle extremes, low solar and geomagnetic activity, Arctic cold-glaciation linked to glacial cycle stage, and geographic risk.

**Key words:** influenza pandemic; zoonosis; risk factor; circadian system; cold stress; immunosuppression; low solar activity; geomagnetism; cosmic rays; cold climate change.

# Introduction

The Little Ice Age (mid-13$^{th}$ to mid-19$^{th}$ centuries) was the coldest period after the Holocene Climate Optimum (HCO, peak glacial cycle temperature), which coincided with five millennia of neoglacial advances that peaked in size mid-study [1], [2]. This period was hallmarked by regional catastrophes associated with cold-glacial climate change, including famine, wars, and epidemics [3], [4]. Dozens of influenza pandemics and regional epidemics, and other diseases, occurred during this period. Pandemics could infect 30-50% of the population within 1-2 years, and were associated with explosive disease spread, and varying mortality rates and geographic extents [5]–[11]. Some 20$^{th}$-21$^{st}$ century influenza pandemic mortality rates were estimated at 1–3% (1918), 0.03% (1968), and 0.001–0.007% (2009) [12].

There is no means of predicting when influenza pandemics could occur because the risk factors associated with pandemics are not well understood [13]. To better prepare for future pandemics (H5N1, H7N9 etc.) we must explore if the spate of zoonoses and pandemic since 1997 were the result of unknown mitigable risk factors. Three categories of risk factors putatively-thematically implicating "immunological susceptibility and induced immunosuppression," and one linked to the study period's stage of the glacial cycle were evident in the literature.

Firstly, *timing risk* has been linked to the extremes of the 11-year sunspot number (SSN) cycle (see Hope-Simpson paragraph). Sunspots represent dark patches of intense magnetic fields that loop through the surface of the sun [14]. An 11-year SSN peak and trough concentration of outbreaks potentially implicates changes in solar magnetic polarity [15] or heliospheric magnetic flux [16], [17]. Theoretically, circadian system cryptochrome repressor proteins whose photoreduction spin chemistry is

magnetoreceptive (a *radical-pair mechanism*), interacting with circadian core molecular clockwork, could offer a means by which solar-/geo-magnetism modulated immuno-inflammatory biology [18]–[20]. The circadian system core molecular clockwork controls the immune and inflammatory systems via oscillatory transcriptional activators (CLOCK–BMAL1) and repressors (Cryptochrome1/2, Period1/2) [21]. Coincidentally, the influenza-A virus (IAV) evolutionarily linked its replication cycle to the circadian system (time of day, winter) [22], [23]. Thus, solar cycle extremes could have dysregulated immune responses, [24], [25] to aid viral entry and replication in immunologically susceptible animals (epizootics), people (zoonosis, family clusters), and populations (epidemics, pandemics).

Secondly, *geographic risk* reflects the prior cited expert reviews [5]–[11]. Geographic risk considers the role of innate immunity single nucleotide polymorphisms (SNPs) in creating immunological susceptibility in people of certain ethnicities (Caucasian, Chinese) to novel-zoonotic IAV infection [26], [27], in regions pertinent to outbreak origination (Europe, North America, Russia, and China). Increased cosmic rays and ionizing radiation have been linked to *immunosuppression* and increased infectious disease mortality [28]–[30]. Peak levels of cosmic ray induced ionization occurred during the Maunder minimum (mid-study) associated with latitudinal and magnetic dipole variations, implicating northern European latitudes and the Far East [31]. Regional-scale immunosuppression could implicate increased cosmic rays directly and indirectly via its climate change impact linked to solar-/geo-magnetism (low cloud cover) [32]. Equine and migrating-avian viral reservoirs and ecology must also be considered in geographic risks.

The literature is devoid of quantitative pandemic risk factor studies associated with solar activity and/or climate change spanning the study period (1500-), beyond timing risk studies (1700-). Therefore thirdly, *climate change risks* reflect shorter-term cold weather influences on seasonal influenza and avian influenza epizootics. Firstly, the degree and duration of *cold stress* dysregulate immune responses [33], [34], implicating key immuno-molecular pathways coopted by IAVs during infection (e.g. Nuclear Factor kappa B, NF-κB) [35], [36]. Secondly, cold weather modulates the formation and dispersion of *infectious aerosols*, their respiratory tract (RT) penetration, and drying out RT mucosa [37]. Thus, low temperature

and relative humidity were inversely correlated with influenza disease burden during cooler-drier winters in temperate regions [38], [39]. A fourth risk factor linked to the mid-study period's stage of the glacial cycle (coldest iciest post-Holocene Climate Optimum period) was evident in the literature (Discussion).

In 1978 Hope-Simpson published a Nature correspondence suggesting 20th century pandemics were associated with sunspot number maxima [40]. A few statistical studies since reported pandemic timing risk associated with the 11-year international sunspot number cycle peaks +/- 1-year (Tapping) [41], and troughs +/- 1-year as well (Ertel, Qu) [42], [43], or sunspot numbers exceeding percentile thresholds (Yeung) [44]. This sunspot cycle timing risk was also demonstrated with SARS-CoV-2 (2019 sunspot number trough) and is claimed for Ebola [45]. Pandemics have also been linked with grand solar minimum periods [46], [47].

Towers, an expert biostatistician, falsified the Tapping, Ertel, and Yeung studies after applying more robust statistical methodologies to their corrected outbreak lists [48]. Qu more recently used Yeung's pandemic list and logistic regression analysis to show that sunspot number maxima and minima +/– 1-year were risk factors. The influenza outbreak consensus lists used by Tapping, Ertel, and Yeung (also Qu) were derived from numerous publications (1927-1998, median 1986). These publications detailed different geographies over different periods using varying pandemic definitions and data sources, which likely resulted in incompleteness, inaccuracy, and uncertainty [5], [6]. Solar-pandemic timing risk study lists either utilized the historian lists as provided (Tapping) or criteria to derive smaller consensus lists (Ertel, Yeung, Qu), meaning valuable outbreak data was discarded. No previous solar activity-pandemic outbreak lists detailed regional epidemics, concurrent epizootics, or geographic origin and extent.

Comprehending the high-level chain of biological events common to all novel-zoonotic IAV infections, irrespective of whether that IAV arose by mutation, recombination, or reassortment [49], aids an immunology orientation to this study. Geographically expansive outbreaks arose when a novel-zoonotic IAV emerged for which a susceptible population (broad demographics) lacked pre-existing protective immunity (neutralizing antibody and/or cellular immunity). At the same time, all novel-zoonotic IAVs

overcame and/or dysregulated immunological defenses (innate and early adaptive immunity), physical (mucosal surfaces), and cellular barriers (cell attachment and entry, intracellular restriction factors) [50]–[52]. The IAV then replicated in the respiratory tract in sufficiently high titers and was transmitted to a second person. This biological journey will be referred to as "Bottleneck-1", and only after this was surmounted could geographically expansive transmission have occurred ("Bottleneck-2") [53].

Influenza pandemics, regional epidemics, concurrent epizootics and their geographic details were compiled from seven expert reviews, and organized into five category groupings. Outbreaks were (re)classified according to WHO Phase 5 and 6 pandemic descriptions based on pooled geographic information. Numerous regression and other statistical methods were used to define risk factors, probabilities, and predictors from among 10 solar-/geo-magnetic activity (*proxied by cosmic ray intensity, 10-Beryllium cosmogenic radionuclide, solar modulation function, sunspot numbers*) and solar electromagnetic activity (*proxied by total solar irradiance*), and climate change variables (*proxied by Northern Hemisphere and Greenland temperatures, Artic sea ice cover, Greenland ice accumulation rate*) spanning 3-5 centuries. All data was geographically relevant to outbreak origination and dissemination and animal-IAV reservoirs. Sixteen polar ice cores were used to benchmark the study period's climate relative to the Holocene Climate Optimum peak glacial cycle temperature 8kyr ago.

# Materials and methods

## Pandemic and epidemic database

Influenza pandemics, regional epidemics and concurrent animal epizootics from 1500-2009 were identified in seven reviews (2001, 2008-2011) by six expert professors [5]–[11]. Key information was summarized from these reviews and 32 pooled review-cited sources, and tabulated into categories defined in S1 Figure A pandemic reflected an expert-reviewer's explicitly stated description of an 'influenza' outbreak, which was confirmed in the pooled literature in ≥2 WHO regions, whereas an epidemic reflected expert descriptions of an 'influenza' outbreak confirmed in one WHO region (≥2 countries, or

126 stated as regional). This classification was consistent with WHO Phase 5 regional epidemic and Phase 6
127 pandemic descriptions [54], thus enabling an objective (re)classification of outbreaks based on pooled
128 geographical information. This method avoided subjective disease severity judgments based on
129 incomplete information, while reflecting that not all outbreaks resulted in severe disease with high
130 mortality that left their mark in the global historical record, especially pre-1700.

131 Pandemic and major regional epidemic ("epidemic") data was pooled for combined and separate analysis,
132 and robustness testing, as follows:

133 1) Category A pandemics (pandemics +/-epizootics/zoonosis plus epidemics with epizootics/zoonosis)
134 (epizootic/zoonosis = epizoo, category = Cat.),
135 2) Cat.B epidemics (epidemics without epizootics/zoonosis),
136 3) Pandemics +/-epizootics (pandemics +/-epizootics/zoonosis),
137 4) Epidemics +/-epizootics (epidemics +/-epizootics/zoonosis).

## 138 Solar activity and climate change data

139 Annually resolved publicly available datasets starting between 1500 and 1700 and ending post-1994, were
140 obtained from the National Oceanic and Atmosphere Administration (NOAA), Laboratory for
141 Atmospheric & Space Physics Interactive Solar Irradiance Data Center, International Association of
142 Geomagnetism and Aeronomy, and WDC-SILSO Royal Observatory of Belgium websites. The following
143 datasets were collected for analysis and benchmarking:

144 *Solar-/geo-magnetic activity related datasets*: international sunspot numbers (SSN data) [55], and group
145 sunspot numbers (GSSN data) [56], cosmic ray intensity (CRI data) [57], solar modulation function (MeV
146 data) [58], 10-Beryllium radionuclide ($^{10}$Be data, see missing data comment in the readme file, Figshare)
147 [59]. Geomagnetic activity index data was also downloaded for correlation analysis (GMA-AA data,
148 1868-) [60], given solar modulated geomagnetism (solar-/geo-magnetism) controls atmospheric cosmic
149 ray entry and ionization [61]. *Solar electromagnetic activity dataset:* total solar irradiance (TSI data) [62].

*Climate change* datasets: Northern Hemisphere temperature (NHT°C data) [63], Greenland ice core derived temperature (GT°C data) [64], Arctic algal growth anomaly (inverse sea ice cover proxy, SIC data) [65], and Greenland ice accumulation rate (IAR data, see $^{10}$Be missing data comment above, same dataset) [59]. All terrestrial-derived datasets were geographically relevant to influenza outbreaks and animal-IAV reservoirs.

Data was provided as, or converted to *anomaly data* relative to the climate reference period mean (RPM), generally the 1961-1990 mean (except SIC and MeV), per the norms of the scientific community for long-term climate change assessments [66]. A negative NHT°C and GT°C anomaly indicated a colder temperature than the 1961-1990 RPM. A negative SIC anomaly indicated less crustal algal growth than at its RPM due to less sunlight reaching the sea floor rocks, corresponding with an increase in sea ice cover [65]. A positive IAR indicated increased Greenland glaciation rates above the RPM. A negative SSN, GSSN, TSI, and MeV anomaly, and a positive CRI and $^{10}$Be indicated solar activity lower than the RPM.

A glacial cycle perspective on outbreak risks was obtained by benchmarking the 11,400-year GT°C dataset against 15 other Polar ice cores, utilizing two-three immutable glacial cycle landmarks. For *analytical and graphical purposes*, the glacial cycle peak temperature closest to the end of the prolonged interglacial rise was termed the Holocene Climate Optimum (HCO); the Little Ice Age (LIA) temperature nadir the lowest post-HCO temperature trough during the LIA period (mid-13$^{th}$-19$^{th}$ centuries). The Last Glacial Maximum (LGM) corresponded with the lowest temperature trough of the last glacial cycle immediately prior to the sustained interglacial temperature rise. The Holocene interglacial was the period between the LGM and HCO. *Benchmarking datasets*: Greenland; (Vinther data) [67], (Alley data) [68], (Buizert, nine different Greenland ice core locations) [69]. Antarctica; (Jouzel data, EPICA Dome C) [70], (Uemura data, Dome Fuji) [71], (Lorius data, Vostok) [72], (Mulvaney data, James Ross Island) [73].

# Basic data analysis

Basic statistical parameters were assessed for each independent variable (IV: number of years, mean,

median, minimum, maximum, standard deviation-SD, confidence intervals). The normality of data distribution was assessed by skewness (within +/-2), and kurtosis (within +/-7) values because all datasets exceeded 300 years [74]. Eleven correlation matrices (1–11-year SMA periods) were produced between ten solar-/geomagnetic and electromagnetic activity and climate change variables (SSN, 10Be, CRI, MeV, TSI, GMA-AA, and NHT°C, GT°C, SIC, IAR). Collinearity was assessed during multiple logistic regression analysis using the variance inflation factor (VIF). For this study, a VIF>10 was considered problematic, a VIF>5 was highly correlated, and a VIF>2.5 was moderately correlated [75].

# Outbreak distribution by solar cycle stage (timing risk factors)

Influenza outbreak distributions across the 11-year solar cycle since 1700 were investigated (Figure 1A) using simple logistic regression. This method was used to derive the probability of an outbreak by solar cycle stage groupings, for SSN, GSSN, and TSI cycles [76]. Investigatory stage groupings comprised the peak +/- 1-year (P01), trough +/- 1-year (T01), and the combined peak and trough +/- 1-year (P01+T01), versus the combined inter-peak-to-trough plus inter-trough-to-peak stages (P_T+T_P) (Figure 1B).

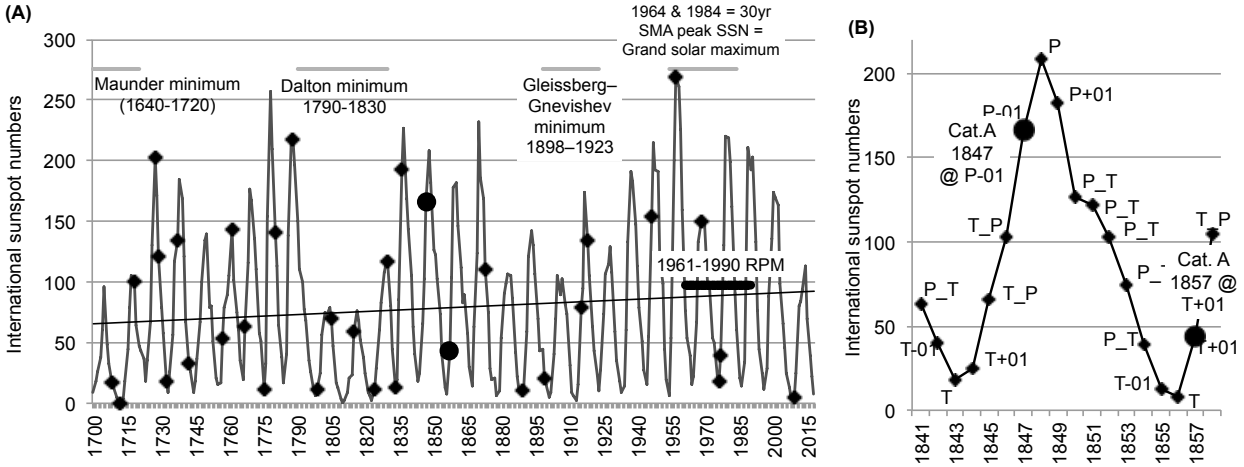


**Figure 1: International sunspot number cycles and influenza outbreaks since 1700. (A)** Sunspot numbers from 1700-2018 depict solar cycles with varying periodicities, including the 11-year Schwabe cycle and other superimposed longer-term "grand solar" cycles that modulated the magnitude of the 11-year Schwabe cycle SSN peaks and troughs. During the Little Ice Age and study period, there were numerous grand solar minimum periods,

192 including the Wolf (1270-1340), Spörer (1390-1550), Maunder (1640-1720), Dalton (1790-1830), and Gleissberg–
193 Gnevishev (1898–1923) minima [77]–[79]. Since the 1957 Solar Cycle-19 SSN peak, all Schwabe cycle peaks have
194 declined, indicating the sun entered a new grand solar minimum period. **(B)** An extracted Schwabe cycle (1843-
195 1856) is used to demonstrate the solar cycle stage classification used to create binary variables for regression
196 analysis. Data citations: Outbreak database reviews [5]–[11]. Publicly available sunspot number data [55].

197 Logistic regressions were estimated according to the following equations:

198 $$ln\left(\frac{p}{1-p}\right) = b_0 + b_1 \cdot D_{P01} + b_2 \cdot D_{T01}$$ (for P01and T01 separately). (1)

199 Where $D_{P01}$ is a dummy variable: 1 for P01, and 0 for all other cycle stages; $D_{T01}$ is a dummy variable: 1
200 for T01, and 0 for all other cycle stage; $b_1$ and $b_2$ are regression coefficients.

201 $$ln\left(\frac{p}{1-p}\right) = b_0 + b_1 \cdot D_{P01T01}$$ (for the combined P01+T01) (2)

202 Where $D_{P01T01}$ is a dummy variable (0 for P_T+T_P, and 1 for T01 and P01); $b_0$ is the intercept, $b_1$ is the
203 dummy variable coefficient. These formulas were used to determine the coefficients $b_1$ or $b_1$ and $b_2$,
204 enabling the determination of the effect of the stage grouping on outbreak probability (increase, decrease,
205 no impact). Cycle stage probabilities and Odds ratios (OR) were then derived.

206 The Fisher's exact test of independence was used to assess differences in solar cycle stage distributions
207 between pandemic +/-epizootics versus epidemic +/-epizootics, for cycles defined by SSN, GSSN, TSI,
208 CRI, and MeV periodicities. This method compared the differences in the proportion of years with an
209 influenza outbreak over key stages of the solar cycle post-1700. Stage comparisons included P01, T01,
210 and P01+T01 versus T_P+P_T, and P+T, and P+T (exact peak plus trough) versus All stages-(P+T). The
211 outbreak proportion was calculated as the number of years with outbreaks multiplied by 100 and divided
212 by the total stage years.

213 # Logistic and linear regression analysis (non-timing risk factors)

214 Three regression methods were utilized to identify non-timing outbreak risk factors, and understand what

factors increased or decreased the probability of an outbreak. Firstly, a simple logistic regression was used to investigate the impact of a single independent variable (IV) or predictor in explaining the variability of the dependent variable (outbreak category), in case the outcome was binary [80] [81]. Logistic regressions were estimated according to the following equation [82]:

$$In\left(\frac{p}{1-p}\right) = b_0 + b \cdot X_i \qquad (3)$$

Where $p$ was the probability that an outbreak existed in a certain year; $Xi$ is one of the IVs (SSN, GSSN, TSI, CRI, MeV, 10Be, NHT°C, GT°C, SIC, and IAR); $ln$ (Ln) denotes the natural logarithm; $b_0$ and $b$ are regression coefficients. Ten logistic regressions based on model (3) were estimated using the raw anomaly and a 2–11-year SMA data (one-sided moving average) from 1500- and 1700-. Data smoothing was used to determine if the predictive utility was improved by removing short-term volatility, and to reflect the sequential increase in Pearson correlation coefficients between 2 and 11 years with solar-/geo-magnetic activity and electromagnetic activity variables, versus climate change variables.

Secondly, it was investigated if the mean number of outbreaks per solar cycle year could be predicted by the cycle mean anomaly, where cycle timelines were defined by SSN, GSSN, TSI, CRI, and MeV trough-to-trough periods (T_T, from 1700-). Simple linear regression was used to check for linear associations between these continuous variables [83]. For each set of cycles defined by SSN, GSSN, TSI, CRI, and MeV, 10 linear regressions were estimated according to the following equation [80]:

$$Y'_i = a_0 + a \cdot \overline{X_i} \qquad (4)$$

Where $Y'_i$ was the predicted mean number of category outbreaks per year for cycle number $i$, $\bar{X}_i$ is an average of the independent variable (one of SSN, GSSN, TSI, CRI, MeV, $^{10}$Be, NHT°C, GT°C, SIC, and IAR) for cycle $i$, $a_0$ and $a$ are corresponding regression coefficients.

Thirdly, multiple logistic regression was conducted to investigate the simultaneous impact of up to eight IV predictors (assessed 1–11-year SMA) plus a SSN P01+T01 dummy variable on the probability of five different categories of influenza outbreaks. A stepwise (SW) backward method was used and 55 models

were assessed based on mathematical criteria. An initial multiple logistic regression equation contained all IVs as follows (from 1700-) [84] [85]:

$$\ln\left(\frac{p}{1-p}\right) = b_0 + b_1 \cdot \mathrm{Dummy_{SSN}} + b_2 \cdot \mathrm{TSI} + b_3 \cdot \mathrm{CRI} + b_4 \cdot \mathrm{MeV} + b_5 \cdot \mathrm{Be10} + b_6 \cdot \mathrm{NHT°C} + b_7 \cdot \mathrm{GT°C} + b_8 \cdot \mathrm{SIC} + b_9 \cdot \mathrm{IAR} \quad (5)$$

Where p is the probability an event existed in a particular year; ln denotes the natural logarithm; $b_0$ and $b_{1\text{-}9}$ are regression coefficients. Predictors were then iteratively removed, and an interim assessment made using the Akaike information criterion (AIC). This was continued until the most reduced model was identified comprising the lowest AIC value, with at least one significant variable ($Pr>|z|<0.050$) plus associated marginal predictors ($Pr>|z|<0.20$, but mainly $Pr>|z|<0.15$).

## Outbreak distribution by variable anomaly quartile groupings

Chi-squared and Fisher's exact tests of independence were used to assess anomaly magnitude and sign quartile grouping proportion differences in outbreaks (1500-, 1700-). Independent variable anomalies were classified into six categories based on percentiles: large, medium, and small negative and positive quartiles. An anomaly below the 25th percentile was considered “low,” above the 75th percentile “large,” and between 25th and 75th percentiles “medium” for both positive and negative anomalies. For each outbreak category, the number of years with and without outbreaks was calculated, from which quartile grouping proportions were calculable in R. Chi-squared (used when the expected frequency ≥5) and Fisher's exact tests (used when the expected frequency <5) of independence were used to compare differences between the observed frequency ($f$o) and expected frequency ($f$e) distributions of outbreaks (proportions) by quartile groupings [86].

## General statistical analysis considerations

This exploratory study involved the use of multiple statistical analyses each with implicit sub-hypotheses using continuous data and fixed outbreaks, without any form of random sampling procedure. No P-value corrections were made for multiple comparisons to ensure the risk of rejecting important discoveries was

minimized, given the catastrophic nature of pandemics and the exploratory-ground breaking scope of this study. Subsequent smaller-scale confirmatory studies with preplanned hypotheses should be conducted to confirm the observed associations [87], [88]. Statistical analyses were conducted using R statistical programming language (version 4.0.2) and Microsoft Excel (Mac). For exploratory science purposes, a 2-sided P-value <0.05 or Pr(>|z-score|) <0.05 was considered statistically "significant."

# Results

## Influenza outbreak database overview

The outbreak database details 49 regionally expansive influenza outbreaks identified within the seven expert reviews, which confirmed geographic extent (n = 49/49), origination (n = 49/49), and concurrent epizootics/zoonosis (n = 21/49). Text confirmation of geographic extent, and other relevant information, was provided by a median of 3.0 expert reviews (range = 1-7, mean = 3.2,) and median of 5.0 review-cited publications (range = 1-9, mean = 4.7) per outbreak. Three outbreaks were removed from the provisional pooled list (n = 52) because geographic extent was unverifiable (1529, 1793, and 1843). No new outbreaks from outside the seven reviews were added. Database summary results are provided in S1 Table. The 49 outbreaks were split into 31 pandemics comprising 15 concurrent epizootics (48%), and 18 regional epidemics comprising 6 concurrent epizootics (33%, Figure 2A). Epizootic frequencies were not significantly different between outbreak categories (Chi-square: $X^2 = 1.1$, $p = 0.30$, $df = 1$). Equine epizootics accounted for 76% (n = 16/21) of all concurrent influenza epizootics (Figure 2B).

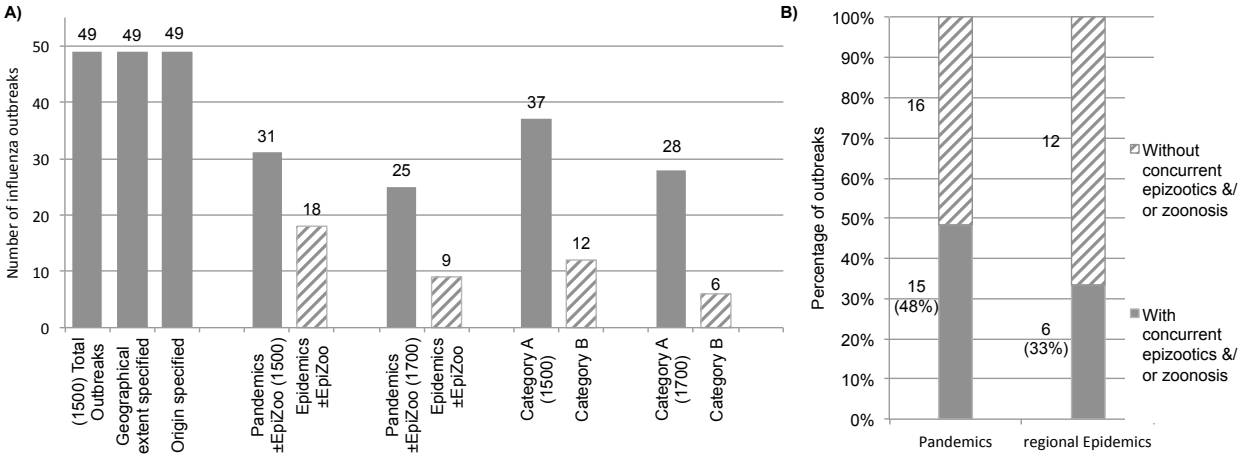


281

282 **Figure 2. Influenza pandemic and regional epidemic outbreaks between 1500 and 2018. (A)** Database summary
283 of the influenza pandemic and major regional epidemics +/-concurrent epizootics/zoonosis, and Cat.A&B outbreaks,
284 from 1500- and 1700- to 2018. **(B)** Summarizes the total number of pandemics and major regional epidemics (1500-
285 2018), and the number and percentage of outbreaks associated with concurrent epizootics/zoonosis (zoonosis proxy).
286 This summary information was derived from the Table S1 (Supplementary materials, Figshare DOI). Outbreak
287 database reviews [5]–[11].

288 Geographic origination was confirmed for 49 of 49 outbreaks, either emphatically (n = 45) or
289 ambivalently (n = 4, Europe or Nth. America?). Where geographic origination was specified, it was
290 concentrated in Europe (EUR n = 21, including Russia n = 5), the Americas (AMR, primarily North
291 America, n = 15), and Asia (n = 8 WPR and SEAR, incl. China n = 4 since 1830) (Figure 3).

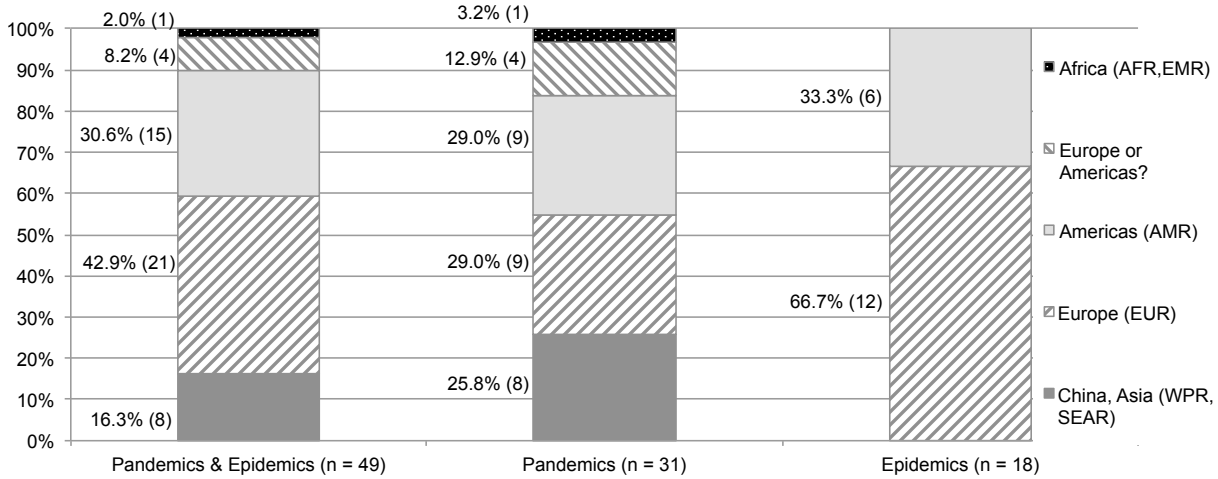


292

**Figure 3. The geographic origination of influenza outbreaks +/-concurrent epizootics/zoonosis.** Summary of the influenza outbreak database detailing the geographic origin of pandemics and major regional epidemics +/- concurrent epizootics/zoonosis between 1500 and 2018. This summary information was derived from the S1 Table (Supplementary materials, Figshare DOI). Outbreak database reviews [5]–[11].

All influenza pandemics from the 1918 Spanish flu, including 1946, 1957, 1968, 1977, and 2009 pandemics, the 1976 swine flu epidemic (USA zoonosis, confirmed human-to-human transmission), as well as the first avian H5N1 (1997) and H7N9 (2013) zoonosis, all occurred within one year of the SSN peak or trough. This SSN peak and trough association was shared by 76% of all outbreaks since 1700 (n = 26/34). Forty-one to 44% of outbreak categories comprising pandemics occurred at the SSN peak +/-1-year and 35-36% at the SSN trough +/-1-year.

Simple logistic regression analysis demonstrated the probability of a pandemic was significantly higher within P01, T01, and P01+T01 stages than P_T+T_P stages of the 11-year solar cycle (n = 24/27 comparisons $P<0.050$, n = 2/27 with P = 0.051 and 0.056, and n = 1/27 with P = 0.08 for cycles defined by SSN, GSSN, and TSI periodicities). These probabilities translated into a mean Odds ratio (OR) of 2.9 (T01), 3.3 (P01), and 3.1 (P01+T01) compared with the P_T+T_P, averaged across all SSN, GSSN, and TSI cycles and categories comprising pandemics, or a mean OR = 3.1 for all SSN, GSSN, TSI, stages and categories comprising pandemics. The S2 Table contains a summary of the beta coefficients, P-values, stage probabilities (p), and Odds ratios (OR) and 95% confidence intervals. The Figure 4 summary information was derived from S2-S4 Tables.

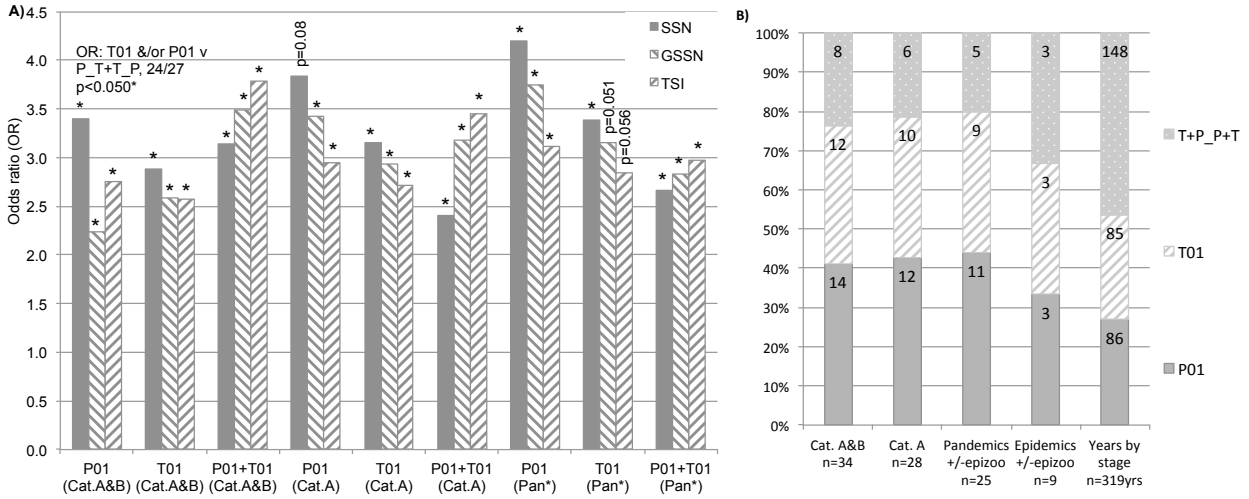


312

313 **Figure 4. Solar cycle stage grouping outbreak probabilities and Odds ratios. (A)** Odds ratios for P01 (peak +/-1
314 year), T01 (trough +/-1 year), and combined P01+T01, compared with the inter-peak-trough plus inter-trough-peak
315 stages (P_T+T_P), for solar cycles defined by SSN, GSSN, and TSI T_T periodicities, for different categories of
316 pandemics (Cat. A&B, Cat. A, and pandemics +/-concurrent epizootics/zoonosis). The Asterix above each P01, T01,
317 and P01+T01 Odds ratio bar indicates a significant difference over P_T+T_P stage probabilities ($p<0.050$). This
318 data was derived from the S2 Table, which in turn was derived from S3 Table. **(B)** The number of influenza
319 outbreaks by SSN cycle stage groupings for different categories of influenza outbreaks and the number of years in
320 each stage grouping (far right bar). These results were derived from the S4 Tables (supplementary materials,
321 Figshare DOI). Data citations: Outbreak database reviews [5]–[11]. Publicly available independent variable data
322 [55], [56], [62].

323 The Fisher's exact test results showed there were no significant differences in solar cycle stage frequency
324 distributions between pandemics and epidemics +/-epizootic (all $P \geq 0.20$, except one $P = 0.12$, S5 Table).

## 325 Simple logistic regression analysis revealed non-timing risks factors

326 There was a higher probability of an outbreak during sustained (1-11yr SMA) cooling (-GT°C, -NHT°C
327 anomalies) and glaciation periods (-SIC crustal algal growth = increased sea ice cover, +IAR anomalies),
328 relative to their respective RPM. Significant negative regression coefficients were obtained between
329 GT°C and Cat.A&B outbreaks (all $B = -0.6$, all $P<0.04$, $n = 48$, 1–11-year SMA, 1500-), and with

NHT°C and epidemics +/-epizootic since 1500 (all B = -2.8 to -3.1, all P = 0.01, n = 18, 1–11-year SMA) and 1700 (all B = -3.4 to -3.6, all P = 0.01, n = 9, 1–11-year SMA). A significant negative coefficient indicates a reduced outbreak probability as the GT°C and/or NHT°C increased above the RPM, and vice versa. Results in this section refer to Table 1 and S6 Table (supplementary materials, Figshare DOI).

**Table 1. Coefficients of simple logistic regression and P-values by outbreak category**

| Outbreak | A&B | Epi* | Epi* | Epi* | Epi* | Epi* | A&B | A | Pan* | Epi* | A&B | Epi* | Epi* | Epi* | Epi* | Epi* | Epi* | Pan* | Epi* | Pan* |
|---|---|---|---|---|---|---|---|---|---|---|---|---|---|---|---|---|---|---|---|---|
| **Start** | **1500** | **1500** | **1700** | **1610** | **1700** | **1700** | **1700** | **1700** | **1700** | **1500** | **1700** | **1700** | **1700** | **1700** | **1610** | **1500** | **1700** | **1610** | **1500** | **1500** |
| **Variable** | **GT°C** | **NHT°** | **NHT°** | **TSI** | **CRI** | **MeV** | **SIC** | **SIC** | **SIC** | **IAR** | **CRI** | **TSI** | **SSN** | **GSSN** | **GSSN** | **Be10** | **Be10** | **TSI** | **MeV** | **MeV** |
| **Raw Data** | -0.6 | -2.8 | -3.4 | -1.6 | 6.1 | -0.01 | -0.9 | -0.9 | -0.8 | 12.5 | | | | | -0.3 | | | 0.8 | | 0.002 |
| | (0.04) | (0.01) | (0.01) | (0.02) | (0.002) | (0.02) | (0.01) | (0.02 | (0.04 | (0.04 | | | | | (0.04) | | | (0.048) | | (0.02) |
| **2yr SMA** | -0.6 | -2.9 | -3.4 | -1.4 | 6.5 | -0.01 | *-0.8* | | | | | | | | | | | | | 0.001 |
| | (0.04) | (0.01) | (0.01) | (0.03) | (0.001) | (0.02) | *(0.052)* | | | | | | | | | | | | | (0.04) |
| **3yr SMA** | -0.6 | -2.9 | -3.4 | -1.4 | 6.6 | -0.01 | | | | | 1.8 | | | | | 1.1 | 1.6 | | | |
| | (0.04) | (0.01) | (0.01) | (0.04) | (0.001) | (0.02) | | | | | (0.04) | | | | | (0.04) | (0.03) | | | |
| **4yr SMA** | -0.6 | -2.9 | -3.4 | -1.4 | 6.6 | -0.01 | -1.0 | | | | 2.0 | -2.5 | | | | | | | | |
| | (0.03) | (0.01) | (0.01) | (0.04) | (0.001) | (0.02) | (0.04) | | | | (0.02) | (0.05) | | | | | | | | |
| **5yr SMA** | -0.6 | -3.0 | -3.5 | -1.4 | 6.7 | -0.01 | -1.0 | | | | 2.2 | -2.7 | -0.02 | -0.4 | -0.3 | | | | | |
| | (0.03) | (0.01) | (0.01) | (0.04) | (0.000) | (0.02) | (0.03) | | | | (0.01) | (0.04) | (0.047) | (0.04) | (0.049 | | | | | |
| **6yr SMA** | -0.6 | -3.0 | -3.5 | -1.5 | 6.7 | -0.01 | -1.1 | | | 41.3 | 2.3 | -2.9 | -0.03 | -0.5 | -0.3 | | *1.7* | | | |
| | (0.03) | (0.01) | (0.01) | (0.03) | (0.000) | (0.01) | (0.03) | | | (0.02 | (0.01) | (0.03) | (0.02) | (0.02) | (0.03) | | *(0.051)* | | | |
| **7yr SMA** | -0.6 | -3.0 | -3.5 | -1.5 | 6.5 | -0.01 | -1.0 | | | | 2.3 | -3.2 | -0.03 | -0.5 | -0.3 | | | | | |
| | (0.03) | (0.01) | (0.01) | (0.03) | (0.000) | (0.01) | (0.047) | | | | (0.01) | (0.02) | (0.01) | (0.02) | (0.04) | | | | | |
| **8yr SMA** | -0.6 | -3.0 | -3.5 | -1.6 | 6.5 | -0.01 | *-1.0* | | | | 2.3 | -3.4 | -0.04 | -0.6 | -0.3 | | | | | |
| | (0.04) | (0.01) | (0.01) | (0.02) | (0.000) | (0.01) | *(0.054)* | | | | (0.02) | (0.02) | (0.01) | (0.02) | (0.03) | | | | | |
| **9yr SMA** | -0.6 | -3.0 | -3.5 | -1.6 | 6.6 | -0.01 | | | | | 2.2 | -3.5 | -0.04 | -0.6 | -0.4 | | | | | |
| | (0.04) | (0.01) | (0.01) | (0.03) | (0.000) | (0.01) | | | | | (0.02) | (0.02) | (0.01) | (0.01) | (0.01) | | | | | |
| **10yr SMA** | -0.6 | -3.1 | -3.5 | -1.6 | 5.9 | -0.01 | | | | | | -3.8 | -0.04 | -0.7 | -0.5 | | | | -0.003 | |
| | (0.04) | (0.01) | (0.01) | (0.03) | (0.002) | (0.01) | | | | | | (0.01) | (0.01) | (0.01) | (0.01) | | | | (0.049) | |
| **11yr SMA** | -0.6 | -3.1 | -3.6 | -1.6 | 6.2 | -0.01 | | | | | | -3.9 | -0.04 | -0.7 | -0.5 | | | | -0.003 | |
| | (0.04) | (0.01) | (0.01) | (0.02) | (0.001) | (0.005 | | | | | | (0.01) | (0.01) | (0.01) | (0.01) | | | | (0.049) | |
| **Years (n)** | 494 | 501 | 301 | 409 | 308 | 302 | 311 | 311 | 311 | 481 | 308 | 319 | 319 | 316 | 406 | 481 | 286 | 409 | 502 | 502 |
| **Outbreak** | 48 | 18 | 9 | 15 | 9 | 9 | 34 | 28 | 25 | 18 | 33 | 9 | 9 | 9 | 15 | 18 | 9 | 28 | 18 | 30 |

Coefficients of simple logistic regression and P-values (bracketed, below) for an array of solar activity and climate change variables (raw data, 2–11-year SMA), and different categories of influenza outbreaks between 1500- or 1700- and up to 2018. This summary results table was derived from R results in S6 Table (supplementary materials, Figshare DOI). Data citations: Outbreak database reviews [5]–[11]. Publicly available independent variable data [55]–[59], [62]–[65].

The Arctic crustal algal growth anomaly (sea ice cover proxy, SIC) raw data yielded significant negative regression coefficients for all categories comprising pandemics since 1700 (all B = -0.8 to -0.9, all P = 0.01-0.04, Cat.A&B n = 34, Cat.A n = 28, pandemic +/-epizootic n = 25), and with Cat.A&B outbreaks

and SIC 4–7-year SMA anomalies (all B = -1.0 to -1.1, all P = 0.03-0.047, n = 34). A negative coefficient indicates a reduced outbreak probability as the SIC crustal algal growth increased above the RPM (meaning less sea ice), and vice versa. A significant positive regression coefficient was obtained with the ice accumulation rate (IAR) anomaly and epidemics +/-epizoo since 1500 (B = 12.5 and 41.3, P = 0.04 and 0.02, n = 18, raw data and 6-year SMA). A positive coefficient indicates an increased outbreak probability as the IAR increased above the RPM (Greenland glacier growth), and vice versa.

There was a higher probability of an outbreak during periods of low solar activity. Significant negative regression coefficients were obtained with epidemics +/-epizoo and TSI since 1610 (all B = -1.4 to -1.6, all P = 0.02-0.04, 1–11-year SMA, n = 15) and 1700 (B = -2.5 to -3.9, P = 0.01-0.05, 4–11-year SMA). Significant negative regression coefficients were also obtained between epidemics +/-epizoo and SSN (all B = -0.02 to -0.04, all P = 0.01-0.047, 5–11-year SMA, n = 9, 1700-), and with GSSN since 1610 (all B = -0.3 to -0.5, all P = 0.01-0.049, 1-year and 5–11-year SMA, n = 15) and 1700 (all B = -0.4 to -0.7, all P = 0.01-0.04, 5-11 year SMA, n = 9). Negative coefficients indicate a decreasing outbreak probability as the TSI, SSN, and GSSN increased above the RPM, and vice versa. The P-value significance level increased with data smoothing for these solar activity-cycle variables (from 5 to 11yr SMA).

Significant positive regression coefficients were yielded between CRI and Cat.A&B (all B = 1.8-2.3, all P = 0.01-0.04, 3–9-year SMA, n = 33) and epidemics +/-epizootics (all B = 5.9-6.7, all P<0.01, 1–11-year SMA, n = 9) since 1700. Significant positive regression coefficients were also obtained for $^{10}$Be and epidemics +/-epizoo since 1500 (B = 1.1, P = 0.04, 3-year SMA, n = 18) and 1700 (B = 1.6, P = 0.03, n = 9, 3-year SMA). A positive coefficient indicated an increasing outbreak probability as the CRI and $^{10}$Be increased above the RPM (low solar-/geo-magnetic activity), and vice versa.

## Simple linear regression analysis confirmed outbreak risk factors

There was a grand mean 0.08-0.11 outbreaks per solar cycle year across all influenza outbreak categories comprising pandemics (SE = 0.01-0.02 years or approximately 16% of their respective means, 1711-

2008). This equated to a mean outbreak interval of 9 years (Cat.A&B), 10.7 years (Cat.A) and 12.1 years (pandemics +/-epizoo), or 1.2, 1.0, and 0.9 outbreaks respectively per mean 11-year solar cycle defined by SSN, GSSN, and TSI T_T periods (Figures 5A and B). Data is detailed in S7 Table.

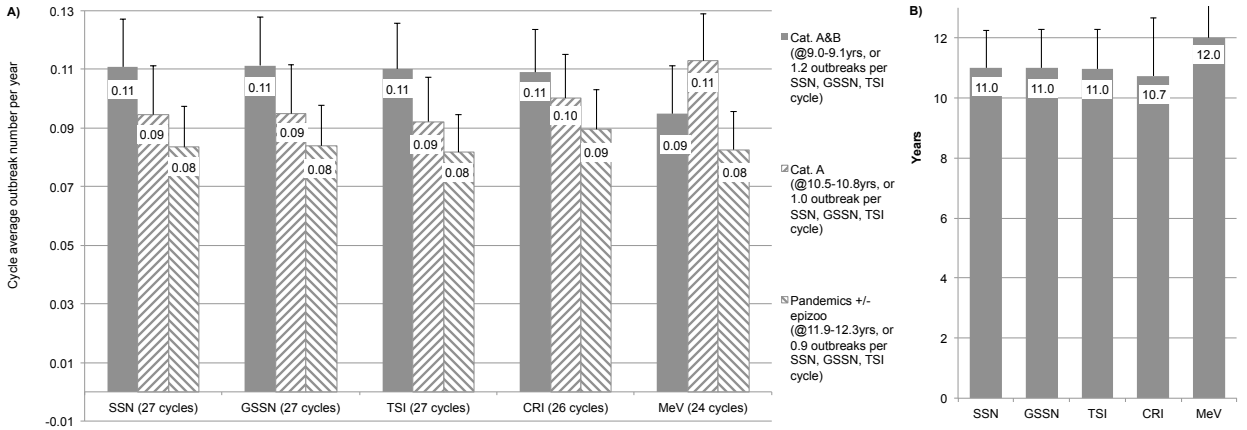


**Figure 5. The mean number of influenza pandemics per year and solar cycle duration. (A)** The mean number of influenza pandemics (different categories) per solar cycle year since 1700 for SSN, GSSN, and TSI cycle T_T periods, with standard error bars (mean of means). The reciprocal of the yearly outbreak rate was the mean interval between outbreaks (detailed in the legend, right of graphic). **(B)** The mean solar cycle duration since 1700 derived from SSN, GSSN, TSI, CRI, and MeV trough-trough periods (years), with standard deviation bars. These graphics were derived from S7 Table (supplementary materials, Figshare DOI). Data citations: Outbreak database reviews [5]–[11]. Publicly available solar activity cycle data used [55]–[58], [62].

Simple linear regression analysis confirmed the ability of cycle mean variable anomalies to predict the mean number of outbreaks per cycle year since 1700. Significant negative regression coefficients were obtained for cycle mean GT°C and mean Cat.A&B outbreaks per year (all B = -0.05 to -0.06, all P = 0.01-0.03, n = 26-27 SSN, GSSN, TSI, and CRI cycle T_T periods, or cycles), and mean pandemics +/-epizoo per cycle year (B = -0.04, P = 0.04, n = 27 TSI cycles). Significant negative regression coefficients were also yielded between mean cycle NHT°C and mean Cat.A&B outbreaks per year (B = -0.15 and -0.16 and P = 0.03 and 0.02, n = 27 and 26 TSI and CRI cycles respectively), and mean epidemics +/-epizootics per year (B = -0.10, P = 0.03, n = 27 TSI cycles). This indicates cycles (esp. CRI, TSI) with a mean GT°C

and NHT°C anomaly greater than the RPM were associated with a lower pandemic and/or epidemic outbreak per cycle year probability, and vice versa. This section refers to Table 2 and S8 Table.

**Table 2. Regression coefficients and P-values (mean cycle variable, mean outbreaks per cycle year).**

| Category | A&B | Pan* | A&B | Epi* | A&B | A | Pan* | Pan* | Epi* | Epi* | A&B | Epi* | Pan* | Epi* |
|---|---|---|---|---|---|---|---|---|---|---|---|---|---|---|
| **Independent** | **GT°C** | **GT°C** | **NHT°C** | **NHT°C** | **SIC** | **SIC** | **SIC** | **IAR** | **IAR** | **Be10** | **CRI** | **CRI** | **MeV** | **TSI** |
| **Solar cycle defined by:** | | | | | | | | | | | | | | |
| SSN (1711-2008, 27 T_T cycles) | -0.05 | | | | -0.11 | | | | | 0.07 | | | | |
| | (0.03) | | | | (0.01) | | | | | (0.03) | | | | |
| GSSN (1711-2008, 27 T_T cycles) | -0.06 | | | | -0.10 | | | | | 0.07 | | | | |
| | (0.01) | | | | (0.01) | | | | | (0.03) | | | | |
| TSI (1712-2008, 27 T_T cycles) | -0.05 | -0.04 | -0.15 | -0.10 | -0.11 | | | | -1.97 | 0.09 | | | | -0.09 |
| | (0.03) | (0.04) | (0.03) | (0.03) | (0.01) | | | | (0.04) | (0.02) | | | | (0.05) |
| CRI (1721-2000, 26 T_T cycles) | -0.05 | | -0.16 | | -0.09 | -0.08 | -0.07 | | | | 0.23 | 0.13 | | |
| | (0.02) | | (0.02) | | (0.01) | (0.03) | (0.04) | | | | (0.03) | (0.01) | | |
| MeV (1709-1997, 24 T_T cycles) | | | | | | | | 2.63 | | | | | 0.0002 | |
| | | | | | | | | (0.04) | | | | | (0.01) | |

Coefficients of simple linear regression are summarized for an array of cycle mean independent variables and the cycle mean number of outbreaks per year for cycles defined by SSN, GSSN, TSI, CRI, and MeV trough-to-trough (T_T) periods since 1700. Regression coefficients are placed above the bracketed P-values. This data summary was derived from the R results in S8 Table (supplementary materials, Figshare DOI). Data citations: Outbreak database reviews [5]–[11]. Publicly available independent variable data [55]–[59], [62]–[65].

Significant negative regression coefficients were obtained between cycle mean SIC and mean Cat.A&B outbreaks per cycle year (all B = -0.09 to -0.11, all P = 0.01, n = 26-27 SSN, GSSN, TSI, and CRI cycles), and with Cat.A and pandemics +/-epizoo outbreaks (B = -0.08 and -0.07, P = 0.03 and 0.04 respectively, n = 26 CRI cycles). A significant positive regression coefficient was obtained between cycle mean IAR and mean pandemics +/-epizootics per cycle year (B = 2.63, p = 0.04, n = 24 MeV cycles). By contrast, a significant negative regression coefficient was yielded between cycle mean IAR and mean epidemics +/-epizootics per cycle year (B = -1,97, p = 0.04, n = 27 TSI cycles).

A significant positive regression coefficient was obtained with mean CRI cycle anomalies and mean Cat.A&B outbreaks per cycle year (B = 0.23, P = 0.03) and with mean epidemics +/-epizoo per cycle year (B = 0.13, P = 0.01) for cycles defined by CRI T_T periods (n = 26). Significant positive regression coefficients were yielded for mean $^{10}$Be cycle anomalies and mean epidemics +/-epizoo per cycle year (all

405 B = 0.07-0.09, all P = 0.02-0.03, n = 27 SSN, GSSN, and TSI cycles). A significant positive coefficient
406 meant there was an increased cycle outbreak rate (per year) as the cycle mean value increased above the
407 RPM, and vice versa. Correspondingly, a significant negative coefficient meant there was a lower
408 outbreak rate (per year) as the cycle mean value increased above the RPM, and vice versa.

## 409 Outbreak distribution by quartile grouping highlights risk factors

410 The mid-study (1750 +/-) broadly coincided with the coldest and lowest solar activity period, while the
411 mid-RPM broadly coincided with the warmest and highest solar activity period, during the study period.
412 The NHT°C anomaly (1500-2000) was at its deepest 30-year SMA trough in 1718 and at its tallest 30-
413 year SMA peak in 1962, while the GT°C anomaly (1500-1993) was at its deepest 30-year SMA trough in
414 1775 and peaked in 1955 (30-year SMA). The $^{10}$Be anomaly (1500-1994) reached its 30-year SMA peak
415 in 1721 (period of lowest solar-/geo-magnetic activity) and its deepest trough in 1964 (period of highest
416 solar-/geo-magnetic activity), while the TSI anomaly (1610-2018) reached its deepest 30-year SMA
417 trough in 1675 and reached its 20$^{th}$ century peak in 1964.

418 The percentage of negative independent variable anomalies and outbreaks associated with negative
419 anomalies are detailed in Figure 6, which summarized co-plots of Cat.A&B outbreaks and all IVs (S9
420 Figure A-J, Supplementary materials). The majority of the temperature (GT°C 74%, NHT°C 90%) and
421 solar activity variables (TSI 71%) were below or above (CRI 81%, $^{10}$Be 68%) their respective 1961-1990
422 RPM. Forty-five of 49 (92%) outbreaks occurred before the RPM and three during the RPM (7.7%).

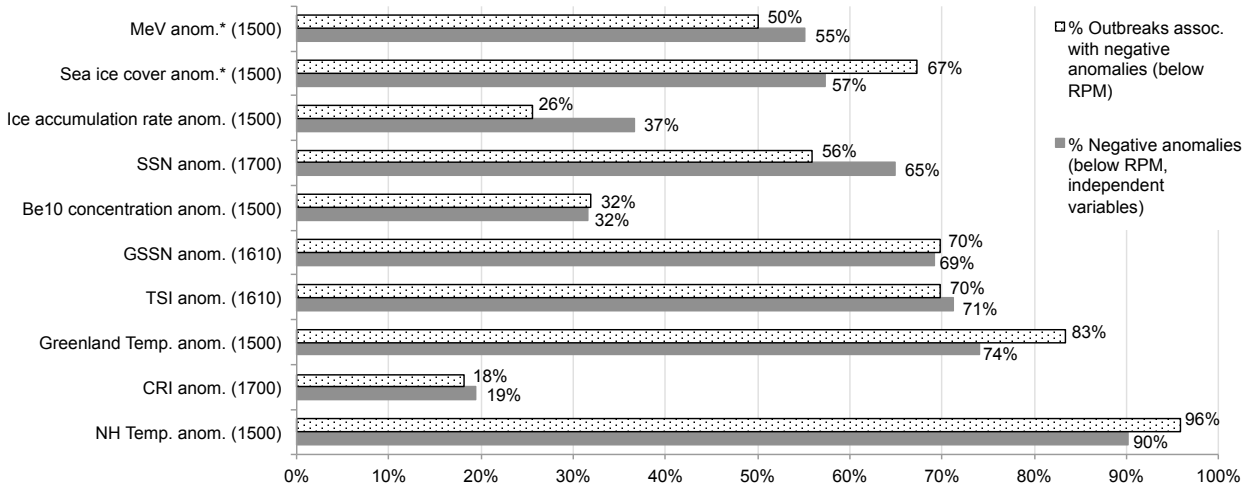


423

424 **Figure 6. Percentage of negative anomalies and outbreaks associated with negative anomalies.** This figure's
425 data summarizes the linear plots for each independent variable and Cat.A&B outbreaks, which are contained in S9
426 Figure A-J (supplementary materials, Figshare DOI). For perspective, the 1961-1990 RPM, by which most variable
427 anomalies were derived, represented a period near the hot-end of a multi-century Arctic and Northern Hemisphere
428 warming phase that started in the early-mid 18th century in the depths of the Little Ice Age (mid-study). Data
429 citations: Outbreak database reviews [5]–[11]. Publicly available independent variable data [55]–[59], [62]–[65].

430 Chi-square ($X^2$) and Fisher's exact (Odds ratio, OR) test values associated with $p<0.05$ ("a significantly
431 higher proportion"), and their degrees of freedom ($X^2$ all df = 1. OR all df = not applicable) are
432 summarized in S10 Table and were derived from S11 Table, which applies to this section. A significantly
433 higher proportion of categories comprising Cat.A outbreaks (SIC, 1500-, 1700-) and epidemics +/-
434 epizootics (GSSN, 1500-) occurred with "*all negative versus all positive*" anomaly quartile-groupings.
435 Significant test values were yielded for "*large negative versus all positive*" quartile-grouping proportions
436 for epidemics +/-epizootics and NHT°C (1700-), TSI (1500-), and MeV (1700-). At the other extreme, a
437 significantly higher proportion of outbreaks occurred with "*large positive versus all negative*" quartile
438 groupings between epidemics +/-epizootics and IAR (1500-) and CRI (1500-, 1700-), and with MeV and
439 pandemics +/-epizootics (1500-).

440 A significantly higher proportion of outbreaks occurred with "*large plus medium negative versus all*

441 *positive*" quartile-groupings for categories comprising pandemics (SIC, 1500, 1700-) and with epidemics
442 +/-epizootics (GSSN, 1500-). At the other extreme, significant test values were obtained for "*large plus*
443 *medium positive versus all negative*" quartile-groupings for categories comprising pandemics (GT°C, SIC
444 IAR, SSN, MeV, 1500- and/or 1700-). A significantly higher proportion of outbreaks occurred with
445 "*large plus medium negative versus large plus medium positive*" anomaly quartile-groupings for
446 Cat.A&B and GT°C (1500-, 1700-), epidemics +/-epizootics with GT°C (1500-) and MeV (1700-), and
447 with Cat.A&B and Cat.A and SIC (1700-).

448 # Multiple logistic regression confirmed outbreak predictors

449 This section reviews the best stepwise models (best models), and all best and short-listed models with ≥1
450 P<0.05 predictor (All-models) across all outbreak categories. This section refers to Table 3 and S12-13
451 Tables. Solar-/geo-magnetic and electromagnetic activity-related variables accounted for the majority of
452 significant and marginal predictors for All-models. Each category best model with the lowest AIC value
453 was achieved when IVs were smoothed between 9 and 11 years.

454 **Table 3. Multiple logistic regression best model and variance inflation factor summary results.**

| **(A) Lowest AIC, Outbreak category Pr(>\|z\|)<0.05, and <0.16** | **β estimate sign: +ve or –ve** | **Cat. A&B** | **Cat. A** | **Pan*** | **Cat. B** | **Epi*** | **(B) Variance Inflation Factor (VIF)** | **Cat. A&B** | **Cat. A** | **Pan*** | **Cat. B** | **Epi *** | **Avg. VIF** |
|---|---|---|---|---|---|---|---|---|---|---|---|---|---|
| SA MAV period | | 11 | 9 | 10 | 11 | 11 | | | | | | | |
| Intercept | -ve | | | | | | | | | | | | |
| 10Be anom. | -ve | | | | 0.12 | 0.07 | 10Be anom. | 3.7 | 2.9 | 3.0 | **93** | 22 | **25** |
| CRI anom. | +ve | | | | 0.04 | | CRI anom. | 12 | 7 | 8 | **634** | 30 | **138** |
| MeV anom. | -ve | | | | | 0.03 | MeV anom. | 3.0 | 2.5 | 2.7 | **159** | 8 | **35** |
| TSI anom. | +ve | | | | 0.10 | 0.04 | TSI anom. | 3.7 | 3.3 | 3.5 | 30 | 9 | **10** |
| NHT°C anom. | +ve | | | | | | NHT°C anom. | 15 | 10 | 11 | 35 | 32 | **20** |
| GT°C anom. | -ve | | | | | 0.10 | GT°C anom. | 5.2 | 4.3 | 4.9 | 61 | 8 | **17** |
| SIC anom. | -ve | 0.16 | | | | | SIC anom. | 3.0 | 3.2 | 3.2 | 11 | 4.5 | **5.0** |
| IAR anom. | +ve | | | | 0.06 | 0.10 | IAR anom. | 1.3 | 1.4 | 1.4 | 11 | 2.2 | **3.4** |
| SSN_dummy_P+T | +ve | 0.04 | 0.049 | 0.04 | | | SSN_dummy_P | 1.0 | 1.0 | 1.0 | 2.1 | 1.2 | **1.3** |
| AIC | | 150.8 | 135.4 | 124. | 31.5 | 52.5 | **Avg. VIF** | **5.3** | **4.0** | **4.4** | **115** | **13** | **28** |
| Cox Snell pseudo- | | 0.03 | 0.02 | 0.02 | 0.08 | 0.06 | | | | | | | |
| Number | | 219 | 229 | 224 | 219 | 219 | | | | | | | |

455 **(A)** Multiple logistic regression best model summaries for each outbreak category (all stepwise, backward method).
456 Each best model summarizes significant and marginal model predictors, provides the sign of the β estimate (positive
457 or negative impact on outbreak probability as the variable increases, and vice versa), and represented the lowest AIC

458 value in its category. **(B)** The variance inflation factor (VIF) was used to assess multi-collinearity. Best model
459 summaries from R are provided in the S12 Table and an All-model summary in S13 Table (supplementary materials,
460 Figshare DOI), which summarize all 55 short-listed models with ≥1 significant variable. Data citations: Outbreak
461 database reviews [5]–[11]. Publicly available independent variable data [55]–[59], [62]–[65].

462 Solar-/geo-magnetic and electromagnetic activity related predictors accounted for between 100%
463 ($Pr(>|z|)<0.05$, 6/6 IVs, n = 5 models) and 69% ($Pr(>|z|)<0.16$, 9/13 IVs, n = 5 models) of all best model
464 predictors, and between 78% ($Pr(>|z|)<0.05$, n = 43/55) and 67% ($Pr(>|z|)<0.2$, n = 80/120) of All-models.
465 The SSN T01+P01 dummy variable was a significant predictor in all three best models and in 31 of 33
466 potential All-model occurrences, over the three categories comprising pandemics ($Pr(>|z|)<0.2$). In
467 contrast, the SSN T01+P01 dummy variable was not a significant or marginal predictor for Cat.B and
468 epidemic +/-epizootic categories in All-models. Contrastingly, CRI featured in 20/22 All-model potential
469 occurrences with Cat.B and epidemics +/-epizootics ($Pr(>|z|)<0.05$). All three significant best model
470 epidemic predictors were solar-/geomagnetic and electromagnetic activity related (CRI, MeV and TSI).

471 Climate change predictors did not feature to the same degree as solar activity related predictors in All-
472 models. There were no significant best model climate change predictors (all $Pr(>|z|) = 0.06\text{-}0.16$, n = 4 of
473 13 IVs), while three of the four marginal climate change predictors were associated with categories
474 comprising epidemics. However, climate change variables accounted for 22% (all $Pr(>|z|)<0.050$, n =
475 12/55) and 33% of All-model predictors (all $Pr(>|z|)<0.2$, n = 40/120), including SIC (n = 14), NHT°C
476 and IAR (n = 10), and GT°C (n = 6) anomalies. Best model and All-model variance inflation factors
477 (VIF) highlighted a complex issue of multi-collinearity with solar activity (CRI, MeV, 10Be, TSI) and
478 climate change predictors (NHT, GTC, SIC, and IAR), especially with epidemic categories (see next).

479 ## Multi-collinearity implicated solar activity correlated climate change

480 Basic analysis confirmed normal data distributions (skewness within +/-2) and peakedness (kurtosis
481 within +/-7) for all independent variables (S14 Table, Supplementary materials). Pearson correlation

coefficients between regression model IVs (plus GMA-AA) are summarized in Figure 7A and 7B. Of 495 correlation permutations assessed 363 (73%) were P<0.001, 40 were p>0.001 and <0.05 (8.1%) and 92 were non-significant (19%). This correlation analysis highlighted medium-to-high correlations involving solar-/geo-magnetism (esp. CRI, $^{10}$Be) and solar electromagnetism (TSI), with climate change variables: NHT°C with CRI, $^{10}$Be, GMA and TSI anomalies; GT°C with CRI, $^{10}$Be, GMA, NHT, SIC and SSN anomalies; SIC with GMA anomalies. These correlations increased with data smoothing (negative r: avg. r = -0.45 increased to r = -0.70, n = 9 comparators. positive r: avg. r = 0.43 increased to r = 0.65, n = 9 comparators, 1 to 11yr SMA (Figure 7A and 7B, S15 Table, Supplementary materials).

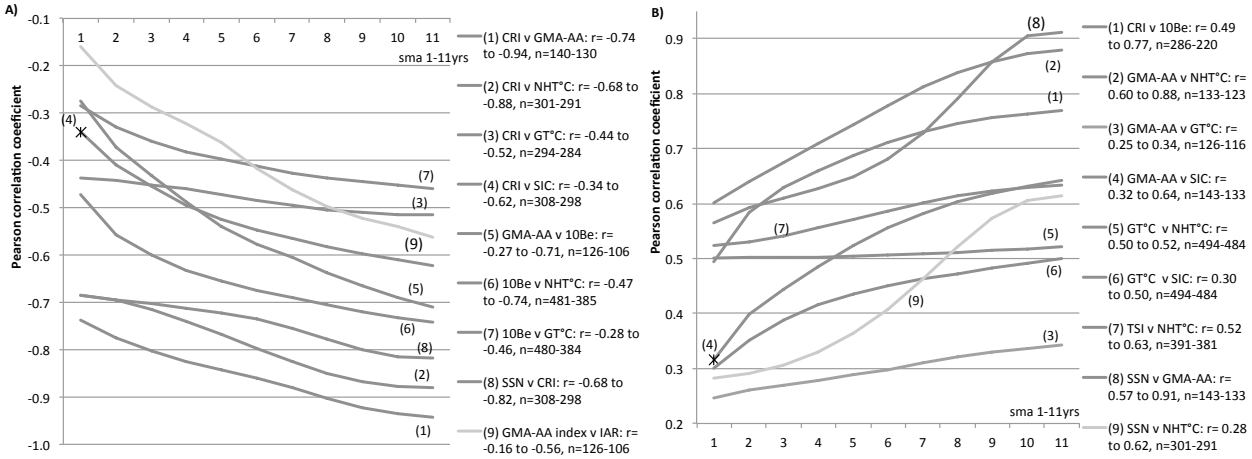


**Figure 7. Pearson correlation coefficients between solar activity and climate change outbreak predictors.** Graphically displayed Pearson correlation coefficients for key solar-/geo-magnetic variables versus solar-/geo-magnetic, solar electromagnetic, and climate change variables, and climate change versus climate change variables (1–11-year SMA, both variables). Correlation coefficients and associated data are provided to the right of each figure **(A)** and **(B)** legend and in the S15 Table (supplementary materials, Figshare DOI). A linear- and scatter-plot of an 18-year SMA $^{10}$Be versus NHT°C raw data anomalies (1406-1994) is provided in S16 Figure (supplementary materials, Figshare DOI). This figure demonstrates that all Little Ice Age grand solar minimum periods paralleled a sustained NHT°C cooling, while these variables counter-tracked each other's large volatilities over decadal to centennial time scales up to the post-RPM period. Data citations: Publicly available independent variable data [55], [57]–[60], [62]–[65].

The best model[1] and All-model[2] mean variance inflation factors for CRI (VIF = 138[1], 41[2]), MeV (VIF = 35[1], 12[2]), 10Be (VIF = 25[1], 6[2]), NHT°C (VIF = 20[1], 13[2]), GT°C (VIF = 17[1], 7[2]), and overall (mean VIF = 28[1], 10[2]) are provided in Table 3B[1] and S13 Table[2] (B). Multi-collinearity was most evident with Cat.B outbreaks (mean VIF = 115[1], 32[2]) and epidemics +/-epizootic (mean VIF = 13[1], 7[2]), two-thirds of which originated in Europe. This level of multi-collinearity indicates potential suppressor-interaction effects between model predictors. This high VIF data (>10) reflects the high-increasing Pearson correlation coefficients (from 1 to 11-year SMA) between the solar-/geo-magnetic proxies, especially CRI (assessed at earth's orbit) and 10Be (Greenland ice core derived), with the terrestrial-derived climate change proxies NHT°C (Greenland ice core derived), SIC (Arctic), and GT°C (Greenland ice core).

# Re-calibrating outbreak risks relative to the Climate Optimum

This section refers to Figure 8, and S17 Table and S18 Figure (16 annotated ice core temperature plots). The Little Ice Age (LIA) GT°C temperature nadir was reached by mid-study in 1761, which occurred 7,771 years after and was -5.9°C below the Holocene Climate Optimum (HCO) peak temperature (6010 BCE) [64]. The Vinther 11,700-year Greenland ice core LIA temperature nadir was reached in 1700, which occurred 7,680 years after and was -4.9°C below the HCO (5980 BCE) [67]. Similarly, the mean of nine Greenland ice cores (Buizert) show the LIA temperature nadir was reached 1802 (SD = 72 years), which occurred a mean 7,307 years after (SD = 920) and was a mean -5.0°C (SD = 1.0°C) below the HCO peak temperature. This mean 5.0°C decline represented 21% of the prior Holocene interglacial increase in absolute terms. During the Holocene interglacial period the temperature increased by a mean 23.1°C in a mean 9,844 years (mean LGM 15,349 BCE and HCO 5,504 BCE) [69].

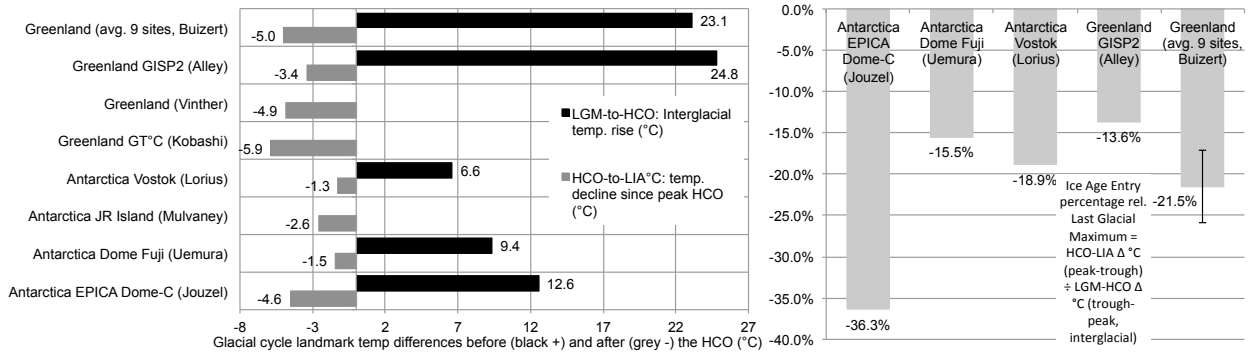


521

522 **Figure 8. The GT°C mid-study climate benchmarked against 15 polar ice cores. (A)** Temperature changes
523 between glacial cycle landmarks are provided for 16 polar ice cores, including the GT°C data used in this outbreak
524 risk factor study. Inter-landmark periods include: (i) the Holocene interglacial period between the Last Glacial
525 Maximum (LGM) and Holocene Climate Optimum (HCO), or the coldest glacial cycle (GC) temperature to the
526 hottest temperature (or anomaly, °C), (ii) the HCO to Little Ice Age (LIA) temperature nadir, or peak glacial cycle
527 temperature to lowest temperature after the HCO during the LIA period. **(B)** The ice age entry percentage
528 corresponds with the temperature decline between the HCO and LIA (by mid-study) divided by the Holocene
529 interglacial temperature increase between the LGM and HCO. See S17 Table for the data table underpinning these
530 graphics (supplementary materials, Figshare DOI). Data citations: Publicly available polar ice core data [64], [67]–
531 [73].

532 From the LIA temperature nadir (1761) to mid-RPM (1975) the GT°C then increased 1.5°C in 214 years,
533 and the Vinther Greenland ice core temperature increased 2.3°C in 260 years from 1700. This means that
534 by 1975 and 1960 Greenland was still 4.4°C and 2.5°C colder than at the HCO 7.8kyr and 7.7kyr
535 beforehand respectively. The Buizert Greenland ice cores showed a mean 2.4°C increase in 178 years
536 from the LIA temperature nadir to the mid-RPM (SD = 0.3°C, n = 9). Despite this warming oscillation,
537 Buizert's nine Greenland ice cores were still a mean 2.6°C lower (SD = 1.0°C) than at the HCO peak
538 temperature 7.5kyr prior, or 11% of their mean Holocene interglacial increase in absolute terms.

539 In Antarctica, the temperature declines between the HCO peak temperature and LIA temperature nadir at
540 Dome-C (Jouzel), Vostok (Lorius), Dome Fuji (Uemura) represented 36%, 19% and 15% respectively of
541 their respective Holocene interglacial increases in absolute terms.

# Discussion

In general, across all analytical methods (1500-, 1610-, 1700-), pandemics (with a SSN P01+T01 trigger) and epidemics (with a +CRI anomaly trigger) were associated with periods of sustained (1-11 years, 11-year cycle means) and/or extreme +/-medium quartile periods of: (1) low solar-/geo-magnetic activity (proxied by +CRI, +10Be, -MeV, -SSN, and -GSSN anomalies) and electromagnetic activity (proxied by –TSI anomalies), and (2) cold-glaciating climate change implicating Greenland (proxied by -GT°C, -SIC-algal growth, and +IAR anomalies) and Northern Hemisphere regions (proxied by -NHT°C anomalies).

Four categories of outbreak risk factors putatively implicating "immunological susceptibility and induced immunosuppression" were identified. These included 11-year solar cycle extremes, low solar and geomagnetic activity, Arctic cold and glaciation (*mid-study was the coldest-iciest period 8-kiloyears after the glacial cycle peak temperature*) and geographic risk (*Europe, North America, Russia, China*). The database and each risk factor are reviewed and compared with prior studies and given relevant context via the literature. The putative means by which risk factors were linked to "immunological susceptibility and regional-scale induced immunosuppression" are also reviewed.

## Influenza outbreak database review

On a comparable basis since 1700, this study's database method confirmed geographical extent for 25 pandemics and nine regional epidemics, and detailed 15 concurrent epizootics/zoonosis (seven reviews). This compared with Tapping's 15-21 pandemics (two reviews), Ertel's 25 pandemics (10 reviews), Yeung's 15 pandemics and possible pandemics (five reviews), while Qu utilized Yeung's uncertain list. This methodology resolved expert review differences in outbreak classifications (9 instances), while eliminating uncertainty for 21 instances of 'possible' pandemics in 157 pooled outbreak assignations. In line with all prior studies and historical records, stated outbreaks may not all have been influenza-A, but could have been other pathogens behaving like and described as influenza. This pathogen-etiology uncertainty was more likely before 1700 due to heterogeneous disease terminologies and a relative

paucity of detailed records by physicians. This inherent uncertainty directed the dual analysis from 1500- and 1700- (3/5 analytical methods started from 1700 anyhow).

A surprise discovery was that since 1500 both pandemics *and* regional epidemics were frequently associated with concurrent influenza epizootics (76% equine associated), which was not significantly different in frequency between these outbreak categories. This concurrent-equivalent epizootic finding between pandemics and epidemics goes against conventional wisdom, in which epidemics were said to be associated with viral mutation of seasonal-endemic IAV subtypes (antigenic drift), while pandemics were said to be associated with zoonosis and/or IAV reassortment (antigenic shift) [6], [10], [89]. This finding indicates some regional epidemics +/-epizootics were different from seasonal-endemic influenza. Alternatively, they could have represented outbreaks whose global spread was thwarted, or represented Europe's special case with epidemics (see discussion on multi-collinearity), or epidemics before 1825 were pandemics incompletely recorded in the global record (mild outbreaks), or combinations thereof.

## Outbreak timing risk factors (solar cycle peaks and troughs)

Pandemics were periodically inescapable on an 11-year solar cycle basis, while solar cycles were relatively predictable. There was roughly one pandemic per 11-year solar cycle since 1700, with three-quarters of these occurring within one year of the cycle peak and trough. There was good agreement between simple and multiple logistic regression in identifying sunspot number P01 and/or T01 solar cycle stages as timing risk factors. Multiple regression analysis confirmed the SSN P01+T01 dummy variable as a significant pandemic predictor in all three best models and 31/33 short-listed models, suggesting SSN cycle extremes +/- 1-year were a pandemic *trigger*. By contrast, significance was not achieved for P01+T01 stages with epidemics (all 22 models), potentially reflecting the smaller numbers of epidemics compared with pandemics (n = 9 -v- 25, 1700-) and/or having different triggers (CRI, see geographic risks). These results confirm Hope-Simpson's original observation on pandemic peak timing, and study conclusions by Tapping, Ertel, Yeung, and Qu claiming a link between SSN extremes and pandemic risk.

The theoretical case for solar-/geo-magnetic modulation of circadian-immuno-inflammatory biology merits consideration in explaining this timing risk data. As introduced, an 11-year SSN P01+T01 concentration of outbreaks potentially implicate changes in solar magnetic polarity and/or heliospheric magnetic flux [14], [17], [61]. Theoretically, magnetoreceptive cryptochrome regulatory proteins (repressors) interacting with circadian core molecular clockwork (CLOCK-BMAL1) offer a means by which geomagnetism could modify immuno-inflammatory biology [18]. Cryptochromes are highly conserved ancient-ubiquitous photoreceptor flavoproteins containing two non-covalently bound chromophores: a redox-active flavin adenine dinucleotide (FAD) and a light-harvesting cofactor. Cryptochrome signaling is tied to the photoreduction of FAD, whose spin chemistry is magnetoreceptive in an effect known as a *radical-pair mechanism*. The feasibility science for magnetoreceptive cryptochrome modulation operating within weak geomagnetic fields was expertly reviewed in the context of bird migration and plant models [19], [20], which highlights its potential for outbreak risk involvement.

# Geographical related outbreak risk factors

This study showed that Europe, North America, Russia, and China originated 81% of all pandemics (n = 25/31, 1500-), while Europe (2/3$^{rd}$) and North America (1/3$^{rd}$) accounted for all epidemics. Historical outbreak reviewer constraints-bias and incomplete record coverage pre-1700 cannot be ruled out. However, other potential causes also exist that implicate Northern Hemisphere (>30-40°N) and Arctic latitudes, and possibly bird migration cruising altitudes over these latitudes. Prior solar activity-pandemic risk factor studies and the seven expert reviews didn't quantitatively assess geographical risks.

**Single nucleotide polymorphisms (SNP)**: One hypothesis is that certain race-ethnicities (Caucasian, Chinese) with innate-/early adaptive- immunity SNP(s) [26], [27], [90], [91], and devoid of preexisting protective-adaptive immunity (Bcell and/or Tcell), were *doubly susceptible* to novel-zoonotic IAV infections. Such people, if in contact with horses, poultry-migrating birds, animal markets and processing [13], [92], could have represented the primary zoonosis doorway and early human-to-human IAV transmission "breeder" population (SNP-family clusters) [93], [94]. In such people-families, Bottleneck-

615 1's biology could have been more readily surmounted if they were rendered immunosuppressed by
616 regional-scale stressors impacting their circadian (P01+T01 solar-/geo-magnetic trigger) and immune
617 systems (cosmic rays, cold stress). Concurrent with surmounting Bottleneck-1's biology, regional viral
618 transmission could have been facilitated in an immunologically susceptible population (Bottleneck-2), if
619 also rendered immunosuppressed (geomagnetism, cosmic rays, cold stress).

620 **Regional modulation of atmospheric cosmic ray entry and ionization**: Cosmic ray intensity was a
621 significant predictor (trigger) in 20/22 All-model potential occurrences for Cat.B and epidemics +/-
622 concurrent epizootics, and in 24/55 significant predictors across all five-outbreak categories. Two-thirds
623 of epidemics originated in Europe and the balance largely in Nth America. Geographical risk could have
624 arisen in these regions associated with differentials in solar- and/or geomagnetism and cosmic ray
625 ionization, in geographical latitudes-altitudes relevant to outbreaks and animal-IAV reservoirs.

626 Magnetic latitude defines a critical threshold (cut-off rigidity) below which cosmic rays of a lower energy
627 cannot enter the atmosphere. Therefore, more cosmic rays penetrate the atmosphere at higher magnetic
628 latitudes and with higher energies, thus increasing northern-regional cosmic-ray ionization [61].
629 Furthermore, variations in earth's magnetic dipole axis were associated with substantial regional
630 differences in geomagnetic field strength and cosmic ray-induced ionization (CRII), with a maximum
631 CRII during the Maunder minimum in Europe (1640-1720). Strong correlations between CRII and low
632 cloud cover also existed (cooling link), limited to the northern Atlantic and Europe, Far East, and
633 Antarctica [31]. Thus, increased CRI/CRII could have impacted geographically relevant regional climate
634 change, in-flight bird risks, and animal-IAV reservoirs and human populations (immunosuppression).

635 **Regional scale cosmic ray induced immunosuppression**: The literature highlights two links between
636 increased cosmic rays and disease biology. Firstly, cosmic rays and ionizing radiation (IR) linked to
637 *immunosuppression* are detailed in the space environment, radiotherapy, and environmental epidemiology
638 literature [28], [29]. Immune response effects (lymphocytes, cytokines, cellular markers) were seen at low
639 chronic exposure rates above and below 1mSv/year (milli-Sievert, international unit of radiation

absorption), and with very low doses of radon gas radiotherapy (0.3 mSv) [29]. The global mean human cosmic radiation dose was estimated at <0.4 mSv/year [95]. This collectively indicates a *low threshold* for immunological sensitivity to cosmic radiation. More generally, natural killer cells (innate immunity) and lymphocytes (adaptive immunity) appear most sensitive to IR [96], [97]. Acute low doses alter lymphocyte and cytokine responses [98], [99], while therapeutic IR modulates important immuno-molecular control pathways [100], which are also coopted by IAVs during infection (NF-κB).

Secondly, there is evidence of *increased disease mortality* in magnetic anomaly regions. Significant correlations exist between annual CRII flux (0.2 mSv/year) and mortality rates in Sao Paulo, including infectious disease mortality. During 11-year solar minima when CRII was high there was a significant increase in mean mortality rates [30]. Sao Paulo resides in the South Atlantic Anomaly (760m above sea level, asl.), or Earth's weakest magnetic field and largest sink for cosmic high-energy particles [101].

For clarity, there is no need to invoke cosmic rays as the cause of IAV mutation underpinning pandemics [43], [46], [47]. This is because IAVs are inherently error-prone during replication (epizootics, zoonosis, epidemics, pandemics, endemics), while the selection pressure imposed by antibody immunity and MHC and HLA system polymorphisms (animal and human genetic diversity in T-cell immune responses) naturally drives viral evolution [25], [50], [102]. The integration of faulty nucleotides occurs at an innate high rate yielding 2–3 nucleotide substitutions per replicated IAV genome [103], [104]. Thus, the opportunity for geographically expansive transmission-optimizing viral evolution is ever-present once a novel-zoonotic IAV replicates itself in sufficient titers to infect another person (or family cluster) for the first time (Bottleneck-1).

**Animal IAV reservoirs**: The source of novel-zoonotic IAVs could also have represented a geographical risk linked to equine and/or avian ecology. *First IAV source*: Forty-three percent (n = 21/49) of influenza outbreaks since 1500 were associated with concurrent epizootics (n = 16/21 equine) (Figure 2B). Morens and Taubenberger tell us, "regardless of geographic locale, equine influenza typically appeared about three weeks before human influenza" [8]. This high concurrency of equine and human outbreaks does not

665 prove zoonosis. However, it does indicate the presence of a novel influenza-like pathogen undergoing
666 epizootic transmission (implying MHC-driven mutation-recombination) in a species placed under
667 *physiological stress* in proximity to humans (transport, work, and war). Human challenge studies with
668 equine influenza virus (EIV) [105], [106] and a review (plus others) confirm the zoonosis potential of
669 EIVs [107].

670 Mongolia spotlights a potential historical geographic hotspot for seeding other horse populations and/or
671 IAV zoonosis. A large horse and wild ass population still exist in Mongolia with preexisting immunity to
672 avian H1, H3, H5, H7, H8, and H10 IAVs introduced during bird migration stop-overs [108], [109]. This
673 indicates cross-species IAV transmission occurred, likely enabled by abundant avian-like α-2,3-sialic acid
674 receptors in the equine upper respiratory tract. It was suggested horses could have historically represented
675 an IAV intermediate host [110]. Such geographic hotspots could have been replicated across Europe,
676 North America, and Eurasia during the Little Ice Age, when horses were more abundant than today.

677 *Second IAV source*: Even though migrating birds did not feature like horses in the concurrent epizootic
678 data, their potential contribution to equine intermediate hosts before zoonosis (IAV mammalianization)
679 and direct zoonosis pre-1900 cannot be ignored. After all, avian IAVs contributed from 1-8 genes to each
680 20th-century pandemic since 1918, and both avian H5N1 and H7N9 zoonosis [8]. Migratory birds are
681 also natural hosts to most IAV strains, making them a dynamic-interchanging viral gene pool reservoir
682 with regional-global reach. Millions of migratory birds biannually flew over northern temperate and high
683 geomagnetic Arctic latitudes (mean altitude 0.5-1.5km, maximum 3–5km asl.) [111], [112]. Thus,
684 physiologically stressed birds carrying IAV strains spent hundreds of hours flying their geomagnetically
685 sensitive physiologies and annually-varying immune systems [113]–[115] through increased cosmic ray
686 levels, varying geomagnetic fields and storms, and much colder temperatures than terrestrial IAV hosts.
687 Bird migration, therefore, increased their circadian-immune system exposure to all outbreak risk factors.

688 Recent avian epizootics with highly pathogenic H5N1 also highlight how Arctic cold winter weather
689 breakouts impacted wild bird migration and over-wintering epidemics in Europe and Eurasia, and how

these diseased birds posed risk to intensively (stressed) farmed animals [116]–[118].

## Indirect outbreak risk factors mediated by solar activity

The same solar-/geo-magnetic activity (proxied by CRI, 10Be, MeV, SSN, and GSSN) and solar electromagnetic activity (proxied by TSI) variable anomalies identified as outbreak risk factors, plus GMA-AA, were also significantly correlated with the Greenland and Northern Hemisphere climate change outbreak risk factors (proxied by NHT°C, GT°C, SIC, IAR), which increased with data smoothing. A strong correlation between the NHT°C raw data and 18-year SMA $^{10}$Be concentration anomaly risk factors (1406-1994) indicates the NHT°C followed sustained changes in solar-/geo-magnetic activity. In fact, all extended cooling phases during the LIA coincided with grand solar minimum periods (S16 Figure, supplementary materials, Figshare DOI).

Multiple regression models highlighted an issue with multi-collinearity, which like the correlation data increased with data smoothing (11yr SMA > raw data). Multi-collinearity strongly implicated solar-/geo-magnetism (CRI >>> MeV >> 10Be) over climate change variables (NHT°C > GT°C), and mainly with epidemic categories (Cat.B > epidemics), which predominated in Europe > North America. Potential model CRI suppressor interactions are indicated by this high multi-collinearity, which is supported by all best model climate change variables being non-significant (all Pr>|z| = 0.051-0.2). This contrasted with GT°C, NHT°C, SIC, and IAR being significant predictors in simple logistic and linear regression analyses.

The above points to a *statistical confirmation* that solar-/geo-magnetic activity was also an indirect outbreak risk factor via its correlated-impact on climate change, explaining the high multi-collinearity. This putative climate change link during the study period is well supported by the literature.

A body of science promulgates a planetary gravitational and inertial influence on the sun (solar dynamo), which control cycles of solar magnetized wind and irradiance emissions. This planetary influence also modulates the Earth–Moon system, which is theorized as a coupled orbital-rotational-energy exchange system (Pattern Recognition in Physics [119]). Magnetized solar wind modulates CRI (at earth's orbit),

and magnetospheric shielding of atmospheric cosmic ray entry (proxied by terrestrial $^{10}$Be and $^{14}$C), which in turn modulates low cloud cover (climate change) [32]. Magnetized solar wind also modulates earth's rate of rotation, which impacts atmospheric circulations (weather systems, climate change) and ocean circulations (heat-energy transfer, climate change), geomagnetism (cosmic ray entry-ionization, dipole axis movement), and periodic tectonic-volcanic activity (climate forcing volcanism) [120]–[124].

In addition to the above described climate change mechanisms, the literature also describes the solar-/geo-magnetic modulation of regional climate change during the Little Ice Age and study period. Strong cooling with +/-extremes of precipitation was observed in the North Atlantic and northern latitudes of Europe [125]–[127], China [128]–[131], and North America [126] [127], plus other regions. This regional climate change impact was mainly correlated with solar-/geo-magnetically modulated cosmogenic radionuclide data ($^{10}$Be, $^{14}$C) and changes in atmospheric-weather circulations (location, phase, intensity). Likewise, Arctic drift ice changes over the last 11,000 years, including the last big LIA advance, were also correlated with cosmogenic radionuclide data ($^{10}$Be, $^{14}$C) [134]. Sustained Arctic sea ice expansion during the LIA also implicated periodic climate-forcing volcanism [135]–[137].

Therefore, in addition to solar-/geo-magnetic activity and cosmic rays putatively impacting circadian-immuno-inflammatory biology (*direct outbreak risk factors*), solar activity correlated climate change also impacted IAV-host biology indirectly via its control over regional weather systems and climate change (*indirect outbreak risk factors*). Periods of colder NHT°C and GT°C (-ve anomalies) and Greenland glaciation (-SIC-algal growth, +IAR anomalies) are assumed to have been reflected regionally in European, Eurasian, and North American weather systems, and in modifying migrating bird habitats, over-wintering, and migration. In so doing, regional-scale cold stress would have immunosuppressed animal and human populations, while cold climate change (modulating temperature-humidity) would have assisted regional-scale infectious aerosol transmission and dried out animal and human respiratory mucosal surfaces to aid viral entry and replication.

# Outbreak risks linked to the glacial cycle stage

739 A fourth risk factor is comprehensible when the study period is given a glacial cycle context relative to
740 the Holocene Climate Optimum (HCO), versus an arbitrary 1961-1990 RPM (per scientific norms) at the
741 *hot end* of a multi-century warming *oscillation* initiated mid-study. By mid-study Greenland was at its
742 coldest post-HCO temperature in nearly 8-kiloyears (mean -4.8°C, n=10 ice cores), or -21% of its prior
743 Holocene interglacial increase (mean +23.3°C) [68], [69]. These post-HCO Greenland temperature
744 declines were comparable to the shorter Kobashi GT°C (-5.9°C) and Vinther (-4.9°C) ice cores (11.5kyr
745 and 11.7kyr respectively) [64], [67]. This devolving-oscillatory temperature decline in Greenland post-
746 HCO as a percentage of the prior interglacial increase was similar to Antarctica (-15% to -36%). After the
747 LIA temperature nadir Greenland then entered a multi-century warming oscillation, which paralleled an
748 unprecedented (in 8kyr) increase in solar activity [138]. However, even by mid-RPM Greenland
749 temperatures were still 2.5°C-4.4°C colder than at the Arctic HCO, meaning the hottest period on record
750 was *history*.

751 The literature confirmed the above data and showed the warmest Arctic period since the Last Glacial
752 Maximum (approx. 18kyr ago) occurred from 8-5kyr ago, with temperatures 2-4°C hotter than today
753 [139]–[141]. The Greenland temperature decline after the HCO paralleled a sustained 40-50 Watt/$m^2$
754 decline in precession modified solar insolation at 60-65°N [142]–[144], or circa 15-times the theoretical
755 radiative-forcing impact of carbon dioxide at today's output level (3 Watts/$m^2$) [145]. Abrupt-periodic
756 Arctic neoglacial advances also started about 5kyr ago, with northeast Greenland perennially ice-locked
757 from 3kyr ago [146], [147]. Five millennia of Arctic glacier advances peaked in size in the *middle of this*
758 *study period* [1], [2]. In Antarctica, the HCO period took place from 11.5-9kyr ago, with a secondary
759 optimum 8-5kyr ago. Periodic post-HCO glacier advances also occurred in Antarctica [141], [148],
760 including the Antarctic Peninsula [149], [150]. Much of this neoglacial ice melted after the LIA
761 temperature nadir and Maunder minimum (1685 = deepest SSN trough in 7.2kyr), along with an
762 unparalleled increase in solar magnetism in 8kyr ($C^{14}$ derived SSN) [138].

763 The above indicates earth *entered a new ice age* after the Holocene Climate Optimum, and the Poles were

near the peak of a solar and geomagnetic activity controlled multi-century warming oscillation at the RPM. Since the HCO peak temperature 8kyr ago, all temperature oscillations switched to a cooling phase, indicating a post-RPM *ice age re-entry* has a certain probability. This probability is supported by solar activity-climate experts who predicted a grand solar minimum trough between 2040 and 2060 and a return to a Little Ice Age-like climate [123], [151]–[155]. This has implications for unmitigated 21st century pandemic influenza risks.

# Conclusion

This environmental immunology study addressed a crucial knowledge gap in influenza pandemic risk factor understanding. Influenza pandemics were triggered by 11-year solar cycle extremes, potentially implicating solar-/geo-magnetic activity repression of magnetoreceptive circadian core molecular clockwork (immune and inflammatory system controller), concomitant with influenza virus replication that evolutionarily coopted the circadian system. Influenza pandemics and regional epidemics were associated with periods of sustained and/or extreme low solar and geomagnetic activity and cold-glaciating climate change (Arctic, Northern Hemisphere), potentially implicating regional-scale cosmic ray and cold-stress induced immunosuppression, and enhanced infectious aerosol transmission and respiratory mucosal drying. Europe[1], North America[1], Russia, and China originated most pandemics and all regional epidemics[1], potentially implicating latitudinal-dipole-altitudinal differentials in cosmic ray induced ionization (immunosuppression, cold climate change), ethnicity-related host immuno-genetics (immunological susceptibility-innate), and equine-avian viral reservoirs and ecology. This collectively aided viral entry and replication in immunologically susceptible animals (epizootic-driven IAV variants), people (zoonosis, family clusters), and populations (pandemics, epidemics). Solar-/geo-magnetic mechanisms of influenza pandemic risk (incl. climate change), and our stage of the glacial cycle are not currently anticipated-mitigated. Prepandemic immunization [156]–[159] utilizing approved influenza vaccine technologies to generate broadly cross-reactive antibody herd immunity [160]–[162]) could mitigate immunological susceptibility and induced immunosuppression (to H5N1, H7N9 etc.) during this

high-risk grand solar minimum period.

# Back matter

## Supplementary materials

All study results are contained within the manuscript and supplementary materials (15 tables and 3 figures), which is available at Figshare (IAV Risk Factor study_Supplementary Materials_2021-08-15):

S1 Table. Influenza pandemic, regional epidemic, and epizootic database summary (1500-2018).

S2 Table. Logistic regression summary results comparing solar cycle stage groupings of outbreaks.

S3 Table. Logistic regression results comparing solar cycle stage groupings of outbreaks (R output).

S4 Table. Number, proportion, and percentage of influenza outbreaks by solar cycle stage grouping.

S5 Table. Solar cycle stage grouping comparisons between pandemics and epidemics.

S6 Table: Simple logistic regression results (2-11yr SMA, non-timing risk factors).

S7 Table. Solar cycle and influenza outbreak per cycle metrics.

S8 Table: Simple linear regression results (cycle mean variable anomaly, cycle mean outbreaks/year).

S9 Figure. Linear plots of independent variables with Cat.A&B influenza outbreaks.

S10 Table. Outbreak proportion and variable anomaly quartile grouping comparisons.

S11 Table. Numbers of outbreak and non-outbreak years by +/- variable quartiles.

S12 Table: Multiple logistic regression best model results (stepwise, backward method).

S13 Table. Multiple logistic regression and variance inflation factor results summary (All-models).

S14 Table. Basic statistical analyses results for independent variables (outbreak risk factors).

S15 Table. Correlation coefficients between solar activity and climate change outbreak predictors.

S16 Figure. Northern Hemisphere temperature -v- 18yr SMA $^{10}$Be conc. anomalies (1406-1994).

S17 Table. Re-calibrated risk factor mid-study period relative to the Holocene Climate Optimum.

S18 Figure. Sixteen polar ice core temperature plots delineating key glacial cycle landmark dates.

## Data availability

A detailed readme description of all database and analytical methods, links to the 26 publicly available datasets used in this study, the preparation of data for analysis, the data and results quality assurance and control procedures, and the R code and R output .txt files are available online (Figshare).

## Acknowledgements

I would like to thank: (1) Oleksii Sukhoi, a freelance statistician (UpWork) for his collaboration with study methodologies, for conducting data analysis in R, and for reviewing the final Excel file and manuscript methods and results for technical accuracy, (2) the National Oceanic and Atmosphere Administration (NOAA), Laboratory for Atmospheric & Space Physics Interactive Solar Irradiance Data Center, International Association of Geomagnetism and Aeronomy, and WDC-SILSO Royal Observatory of Belgium and their contributing scientists for providing the study data.

# References

[1] O. N. Solomina *et al.*, "Glacier fluctuations during the past 2000 years," *Quat. Sci. Rev.*, vol. 149, 2016, doi: 10.1016/j.quascirev.2016.04.008.

[2] O. N. Solomina *et al.*, "Holocene glacier fluctuations," *Quat. Sci. Rev.*, vol. 111, Mar. 2015, doi: 10.1016/j.quascirev.2014.11.018.

[3] A. J. McMichael, "Insights from past millennia into climatic impacts on human health and survival," *Proc. Natl. Acad. Sci.*, vol. 109, no. 13, 2012, doi: 10.1073/pnas.1120177109.

[4] D. D. Zhang, P. Brecke, H. F. Lee, Y.-Q. He, and J. Zhang, "Global climate change, war, and population decline in recent human history," *Proc. Natl. Acad. Sci.*, vol. 104, no. 49, 2007, doi: 10.1073/pnas.0703073104.

[5] D. M. Morens and J. K. Taubenberger, "Pandemic influenza: certain uncertainties," *Rev. Med. Virol.*, vol. 21, no. 5, 2011, doi: 10.1002/rmv.689.

[6] S.-E. Mamelund, "Influenza, Historical," in *International Encyclopedia of Public Health*, Elsevier, 2008.

[7] J. K. Taubenberger and D. M. Morens, "Pandemic influenza - including a risk assessment of H5N1," *OIE Rev. Sci. Tech.*, vol. 28, no. 1, 2009, doi: 10.20506/rst.28.1.1879.

[8] D. M. Morens and J. K. Taubenberger, "Historical thoughts on influenza viral ecosystems, or behold a pale horse, dead dogs, failing fowl, and sick swine," *Influenza Other Respi. Viruses*, vol. 4, no. 6, 2010, doi: 10.1111/j.1750-2659.2010.00148.x.

[9] B. Lina, "History of Influenza Pandemics," in *Paleomicrobiology*, Berlin, Heidelberg: Springer Berlin Heidelberg, 2008.

[10] C. W. Potter, "A history of influenza," in *Journal of Applied Microbiology*, 2001, vol. 91, no. 4, doi: 10.1046/j.1365-2672.2001.01492.x.

[11] E. Tognotti, "Influenza pandemics: A historical retrospect," *J. Infect. Dev. Ctries.*, vol. 3, no. 5,

2009, doi: 10.3855/jidc.239.

[12] CDC, "Estimates of pandemic influenza mortality (20th-21st centuries)." https://www.cdc.gov/flu/spotlights/pandemic-global-estimates.htm.

[13] K. A. Harris *et al.*, "Epidemiological Risk Factors for Animal Influenza A Viruses Overcoming Species Barriers," *EcoHealth*, vol. 14, no. 2. Springer New York LLC, 2017, doi: 10.1007/s10393-017-1244-y.

[14] D. H. Hathaway, "The solar cycle," *Living Rev. Sol. Phys.*, vol. 12, no. 1, Dec. 2015, doi: 10.1007/lrsp-2015-4.

[15] S. Oh and Y. Yi, "Variations in Solar Parameters and Cosmic Rays with Solar Magnetic Polarity," *Astrophys. J.*, vol. 840, no. 1, 2017, doi: 10.3847/1538-4357/aa6c62.

[16] C. Lowder, J. Qiu, and R. Leamon, "Coronal Holes and Open Magnetic Flux over Cycles 23 and 24," *Sol. Phys.*, vol. 292, no. 1, 2017, doi: 10.1007/s11207-016-1041-8.

[17] M. L. Goelzer, C. W. Smith, N. A. Schwadron, and K. G. McCracken, "An analysis of heliospheric magnetic field flux based on sunspot number from 1749 to today and prediction for the coming solar minimum," *J. Geophys. Res. Sp. Phys.*, vol. 118, no. 12, 2013, doi: 10.1002/2013JA019404.

[18] V. Zaporozhan and A. Ponomarenko, "Mechanisms of geomagnetic field influence on gene expression using influenza as a model system: Basics of physical epidemiology," *Int. J. Environ. Res. Public Health*, vol. 7, no. 3, pp. 938–965, 2010, doi: 10.3390/ijerph7030938.

[19] C. T. Rodgers and P. J. Hore, "Chemical magnetoreception in birds: The radical pair mechanism," *Proceedings of the National Academy of Sciences of the United States of America*, vol. 106, no. 2. 2009, doi: 10.1073/pnas.0711968106.

[20] I. A. Solov'yov, D. E. Chandler, and K. Schulten, "Magnetic field effects in Arabidopsis thaliana cryptochrome-1," *Biophys. J.*, vol. 92, no. 8, 2007, doi: 10.1529/biophysj.106.097139.

[21] S. Hergenhan, S. Holtkamp, and C. Scheiermann, "Molecular Interactions Between Components of the Circadian Clock and the Immune System," *Journal of Molecular Biology*, vol. 432, no. 12. Academic Press, 2020, doi: 10.1016/j.jmb.2019.12.044.

[22] C. Scheiermann, J. Gibbs, L. Ince, and A. Loudon, "Clocking in to immunity," *Nature Reviews Immunology*, vol. 18, no. 7. Nature Publishing Group, 2018, doi: 10.1038/s41577-018-0008-4.

[23] G. Mazzoccoli, M. Vinciguerra, A. Carbone, and A. Relógio, "The circadian clock, the immune system, and viral infections: The intricate relationship between biological time and host-virus interaction," *Pathogens*, vol. 9, no. 2. MDPI AG, 2020, doi: 10.3390/pathogens9020083.

[24] P. Gaur, A. Munjal, and S. K. Lal, "Influenza virus and cell signaling pathways," *Medical Science Monitor*, vol. 17, no. 6. International Scientific Literature Inc., 2011, doi: 10.12659/MSM.881801.

[25] M. Schmolke, D. Viemann, J. Roth, and S. Ludwig, "Essential Impact of NF-κB Signaling on the H5N1 Influenza A Virus-Induced Transcriptome," *J. Immunol.*, vol. 183, no. 8, 2009, doi: 10.4049/jimmunol.0804198.

[26] A. Nogales and M. L. Dediego, "Host single nucleotide polymorphisms modulating influenza A virus disease in humans," *Pathogens*, vol. 8, no. 4. MDPI AG, 2019, doi: 10.3390/pathogens8040168.

[27] A. C. Arcanjo, G. Mazzocco, S. F. de Oliveira, D. Plewczynski, and J. P. Radomski, "Role of the host genetic variability in the influenza A virus susceptibility," *Acta Biochimica Polonica*, vol. 61, no. 3. Acta Biochimica Polonica, 2014, doi: 10.18388/abp.2014_1858.

[28] R. Fernandez-Gonzalo, S. Baatout, and M. Moreels, "Impact of particle irradiation on the immune system: From the clinic to mars," *Frontiers in Immunology*, vol. 8. Frontiers Research Foundation, 2017, doi: 10.3389/fimmu.2017.00177.

[29] K. Lumniczky *et al.*, “Low dose ionizing radiation effects on the immune system,” *Environ. Int.*, vol. 149, 2021, doi: 10.1016/j.envint.2020.106212.

[30] C. L. Z. Vieira *et al.*, “Long-term association between the intensity of cosmic rays and mortality rates in the city of Sao Paulo,” *Environ. Res. Lett.*, vol. 13, no. 2, 2018, doi: 10.1088/1748-9326/aaa27a.

[31] G. A. Kovaltsov and I. G. Usoskin, “Regional cosmic ray induced ionization and geomagnetic field changes,” *Adv. Geosci.*, vol. 13, 2007, doi: 10.5194/adgeo-13-31-2007.

[32] I. G. Usoskin, M. Schüssler, S. K. Solanki, and K. Mursula, “Solar activity, cosmic rays, and Earth’s temperature: A millennium-scale comparison,” *J. Geophys. Res. Sp. Phys.*, vol. 110, no. A10, 2005, doi: 10.1029/2004JA010946.

[33] E. F. Foxman *et al.*, “Temperature-dependent innate defense against the common cold virus limits viral replication at warm temperature in mouse airway cells,” *Proc. Natl. Acad. Sci. U. S. A.*, vol. 112, no. 3, 2015, doi: 10.1073/pnas.1411030112.

[34] J. W. Castellani, I. K. M. Brenner, and S. G. Rhind, “Cold exposure: Human immune responses and intracellular cytokine expression,” in *Medicine and Science in Sports and Exercise*, 2002, vol. 34, no. 12, doi: 10.1097/00005768-200212000-00023.

[35] J. R. Roberts, P. A. Rowe, and A. G. Demaine, “Activation of NF-κB and MAP kinase cascades by hypothermic stress in endothelial cells,” *Cryobiology*, vol. 44, no. 2, 2002, doi: 10.1016/S0011-2240(02)00018-4.

[36] T. Arai *et al.*, “Hypothermia augments NF-kappaB activity and the production of IL-12 and IFN-gamma,” *Allergol. Int.*, vol. 57, no. 4, 2008, doi: 10.2332/allergolint.O-08-532.

[37] C. Fuhrmann, “The effects of weather and climate on the seasonality of influenza: What we know and what we need to know,” *Geography Compass*, vol. 4, no. 7. 2010, doi: 10.1111/j.1749-8198.2010.00343.x.

[38] K. Jaakkola *et al.*, “Decline in temperature and humidity increases the occurrence of influenza in cold climate,” *Environ. Heal. A Glob. Access Sci. Source*, vol. 13, no. 1, 2014, doi: 10.1186/1476-069X-13-22.

[39] S. Caini, P. Spreeuwenberg, G. Donker, J. Korevaar, and J. Paget, “Climatic factors and long-term trends of influenza-like illness rates in The Netherlands, 1970–2016,” *Environ. Res.*, vol. 167, 2018, doi: 10.1016/j.envres.2018.07.035.

[40] R. E. Hope-Simpson, “Sunspots and flu: A correlation [1],” *Nature*, vol. 275, no. 5676. 1978, doi: 10.1038/275086a0.

[41] K. F. Tapping, R. G. Mathias, and D. L. Surkan, “Influenza pandemics and solar activity,” 2001. [Online]. Available: https://www.researchgate.net/publication/265988168_Influenza_pandemics_and_solar_activity.

[42] S. Ertel, “Influenza pandemics and sunspots - Easing the controversy,” *Naturwissenschaften*, vol. 81, no. 7, 1994, doi: 10.1007/BF01131945.

[43] J. Qu, “Is sunspot activity a factor in influenza pandemics?,” *Reviews in Medical Virology*, vol. 26, no. 5. John Wiley and Sons Ltd, 2016, doi: 10.1002/rmv.1887.

[44] J. W. K. Yeung, “A hypothesis: Sunspot cycles may detect pandemic influenza A in 1700-2000 A.D.,” *Med. Hypotheses*, vol. 67, no. 5, 2006, doi: 10.1016/j.mehy.2006.03.048.

[45] J. Qu and Z. Gao, “Sunspot Activity, Influenza and Ebola Outbreak Connection,” *J. Astrobiol. Outreach*, vol. 4, no. 2, 2016, doi: 10.4172/2332-2519.1000154.

[46] W. NC, E. J. Steele, W. M, G. Tokoro, M. Fernando, and J. Qu, “Sunspot Cycle Minima and Pandemics: The Case for Vigilance?,” *J. Astrobiol. Outreach*, vol. 05, no. 02, 2017, doi: 10.4172/2332-2519.1000159.

[47] C. E. Navia, "On The Occurrence of Historical Pandemics During The Grand Solar Minima," *Eur. J. Appl. Phys.*, vol. 2, no. 4, 2020, doi: 10.24018/ejphysics.2020.2.4.11.

[48] S. Towers, "Sunspot activity and influenza pandemics: A statistical assessment of the purported association," *Epidemiology and Infection*, vol. 145, no. 13. Cambridge University Press, 2017, doi: 10.1017/S095026881700173X.

[49] W. Shao, X. Li, M. U. Goraya, S. Wang, and J. L. Chen, "Evolution of influenza a virus by mutation and re-assortment," *International Journal of Molecular Sciences*, vol. 18, no. 8. MDPI AG, 2017, doi: 10.3390/ijms18081650.

[50] M. Schmolke and A. García-Sastre, "Evasion of innate and adaptive immune responses by influenza A virus," *Cellular Microbiology*, vol. 12, no. 7. 2010, doi: 10.1111/j.1462-5822.2010.01475.x.

[51] C. J. Warren and S. L. Sawyer, "How host genetics dictates successful viral zoonosis," *PLoS Biology*, vol. 17, no. 4. Public Library of Science, 2019, doi: 10.1371/journal.pbio.3000217.

[52] R. C. Mettelman and P. G. Thomas, "Human Susceptibility to Influenza Infection and Severe Disease," *Cold Spring Harb. Perspect. Med.*, 2020, doi: 10.1101/cshperspect.a038711.

[53] M. Richard, M. De Graaf, and S. Herfst, "Avian influenza A viruses: From zoonosis to pandemic," *Future Virology*, vol. 9, no. 5. Future Medicine Ltd., 2014, doi: 10.2217/fvl.14.30.

[54] World Health Organization, "WHO Pandemic phase descriptions and main actions by phase." https://www.who.int/influenza/resources/documents/pandemic_phase_descriptions_and_actions.pdf.

[55] SILSO World Data Center, "Sunspot Number and Long-term Solar Observations, Royal Observatory of Belgium, on-line Sunspot Number catalogue," *Sunspot Index and Long-term Observations (SILSO), World Data Center*, 2021. http://www.sidc.be/silso/DATA/SN_y_tot_V2.0.txt (accessed Mar. 03, 2020).

[56] SILSO, "Sunspot Number and Long-term Solar Observations, Royal Observatory of Belgium, on-line Sunspot Number catalogue," 2020. http://www.sidc.be/silso/DATA/GroupNumber/GNbb2_y.txt (accessed Mar. 03, 2020).

[57] I. G. Usoskin et al., "doi:10.1029/2002JA009343. CDR Contribution Series # 2008-013: Cosmic Ray Intensity Reconstruction, 2008. This CDR was downloaded from the NOAA National Climatic Data Center." https://www.ncdc.noaa.gov/paleo/study/6101 (accessed Oct. 03, 2020).

[58] R. Muscheler et al., "doi:10.1016/j.quascirev.2006.07.012. CDR Contribution Series # 2008-024: Radionuclide-based Solar Activity Reconstructions for the Last Millennia, 2008. This CDR was downloaded from the NOAA National Climatic Data Center," 2008. https://www.ncdc.noaa.gov/paleo/study/6102 (accessed Feb. 06, 2019).

[59] A. M. Berggren et al., "doi:10.1029/2009GL038004. CDR Contribution Series # 2009-154: North GRIP - 600 Year Annual 10Be Data, 2009. This CDR was downloaded from the NOAA National Climatic Data Center." https://www.ncdc.noaa.gov/paleo/study/8618 (accessed Feb. 05, 2019).

[60] P. N. Mayaud, "DOI 10.1029/ja077i034p06870. Data: Global index, Latest AA* listing of Major Magnetic Storms, 2019. Dataset provided by the International Association of Geomagnetism and Aeronomy. Downloaded from the NOAA National Centers for Environmental Information." ftp://ftp.ngdc.noaa.gov/STP/GEOMAGNETIC_DATA/AASTAR/aaindex (accessed Feb. 10, 2019).

[61] F. J. Pavón-Carrasco, M. Gómez-Paccard, S. A. Campuzano, J. F. González-Rouco, and M. L. Osete, "Multi-centennial fluctuations of radionuclide production rates are modulated by the Earth's magnetic field," *Sci. Rep.*, vol. 8, no. 1, 2018, doi: 10.1038/s41598-018-28115-4.

[62] T. Kopp, G., Dudok de Wit et al, "doi:10.1002/2016GL071866, Dataset: Historical Total Solar Irradiance Reconstruction, Time Series, 2017. This dataset downloaded from the Laboratory for

Atmospheric and Space Physics Interactive Solar IRradiance Data Center." https://lasp.colorado.edu/lisird/data/historical_tsi/ (accessed Oct. 03, 2020).

[63] T. Kobashi et al, "doi: 10.5194/cp-9-2299-2013. CDR: Northern Hemisphere 4000 Year Temperature Reconstructions, 2013. This CDR was downloaded from the NOAA National Climatic Data Center." https://www.ncdc.noaa.gov/paleo-search/study/15535 (accessed Feb. 05, 2019).

[64] T. Kobashi et al., "doi: 10.1038/s41598-017-01451-7. CDR: Greenland 11,500 Year Temperature Reconstruction, 2017. This CDR was downloaded from the NOAA National Climatic Data Center." https://www.ncdc.noaa.gov/paleo-search/study/22057 (accessed Feb. 05, 2019 and Apr. 03, 2021).

[65] J. Halfar et al., "doi: 10.1073/pnas.1313775110. CDR: Arctic Northwest Atlantic 646 Year Coralline Algae Sea Ice Record, 2013. This CDR was downloaded from the NOAA National Climatic Data Center." https://www.ncdc.noaa.gov/paleo/study/15454 (accessed Feb. 06, 2019).

[66] WMO, "WMO Guidelines on the Calculation of Climate Normals," WMO-No. 1203, 2017. [Online]. Available: https://library.wmo.int/doc_num.php?explnum_id=4166.

[67] B. M. Vinther et al, "doi:10.1038/nature08355. CDR series # 2011-053: Greenland Ice Sheet Holocene d18O, Temperature, and Surface Elevation, 2011. This CDR was downloaded from the NOAA National Climatic Data Center." https://www.ncdc.noaa.gov/paleo-search/study/11148 (accessed Apr. 02, 2021).

[68] R. B. Alley, "CDR Series #2004-013: GISP2 Ice Core Temperature and Accumulation Data, 2004. This CDR was downloaded from the NOAA National Climatic Data Center." https://www.ncdc.noaa.gov/paleo/study/2475 (accessed Apr. 02, 2021).

[69] C. Buizert et al., "doi: 10.1002/2017GL075601. CDR: Greenland 22,000 Year Seasonal Temperature Reconstructions, 2018. This CDR was downloaded from the NOAA National Climatic Data Center." https://www.ncdc.noaa.gov/paleo-search/study/23430 (accessed Apr. 03, 2021).

[70] J. Jouzel et al., "https://doi.org/10.1038/316591a0. CDR: Vostok - Deuterium Data and Temperature Reconstruction, 1985. This CDR was downloaded from the NOAA National Climatic Data Center." https://www.ncdc.noaa.gov/paleo/study/6080 (accessed Apr. 02, 2021).

[71] R. Uemura et al., "doi: 10.5194/cp-8-1109-2012. CDR Series # 2012-112: Dome Fuji 360KYr Stable Isotope Data and Temperature Reconstruction, 2012. This CDR was downloaded from the NOAA National Climatic Data Center." https://www.ncdc.noaa.gov/paleo-search/study/13121 (accessed Apr. 02, 2021).

[72] C. Lorius et al., "https://doi.org/10.1038/316591a0. CDR: Vostok - Deuterium Data and Temperature Reconstruction, 1985. This CDR was downloaded from the NOAA National Climatic Data Center." https://www.ncdc.noaa.gov/paleo-search/study/2426 (accessed Apr. 02, 2021).

[73] R. Mulvaney et al., "DOI: 10.1038/nature11391. CDR: James Ross Island Ice Core 14,000 Year Deuterium Temperature Data, 2013. This CDR was downloaded from the NOAA National Climatic Data Center." https://www.ncdc.noaa.gov/paleo/study/13954 (accessed Apr. 02, 2021).

[74] H.-Y. Kim, "Statistical notes for clinical researchers: assessing normal distribution (2) using skewness and kurtosis," *Restor. Dent. Endod.*, vol. 38, no. 1, 2013, doi: 10.5395/rde.2013.38.1.52.

[75] Stephanie Glen, "'Variance Inflation Factor,'" *From StatisticsHowTo.com: Elementary Statistics for the rest of us!* https://www.statisticshowto.com/variance-inflation-factor/.

[76] G. Tripepi, K. J. Jager, V. S. Stel, F. W. Dekker, and C. Zoccali, "How to deal with continuous and dichotomic outcomes in epidemiological research: Linear and logistic regression analyses," *Nephron - Clin. Pract.*, vol. 118, no. 4, 2011, doi: 10.1159/000324049.

[77] I. G. Usoskin, S. K. Solanki, and G. A. Kovaltsov, "Grand minima and maxima of solar activity: New observational constraints," *Astron. Astrophys.*, vol. 471, no. 1, 2007, doi: 10.1051/0004-

6361:20077704.

[78] I. G. Usoskin *et al.*, "The Maunder minimum (1645–1715) was indeed a grand minimum: A reassessment of multiple datasets," *Astron. Astrophys.*, vol. 581, Sep. 2015, doi: 10.1051/0004-6361/201526652.

[79] B. Komitov and V. Kaftan, "The sunspot cycle no. 24 in relation to long term solar activity variation," *J. Adv. Res.*, vol. 4, no. 3, May 2013, doi: 10.1016/j.jare.2013.02.001.

[80] R. M. Warner, *Applied statistics: From bivariate through multivariate techniques (2nd ed.).*, 2nd ed. Sage Publications, Inc., 2013.

[81] S. Sperandei, "Understanding logistic regression analysis," *Biochem. Medica*, vol. 24, no. 1, 2014, doi: 10.11613/BM.2014.003.

[82] B. G. Tabachnick and L. S. Fidell, *Using Multivariate Statistics*, 7th ed. New York: Harper Collins College Publisher, 2007.

[83] J. F. Hair, W. C. Black, B. J. Babin, and R. E. Anderson, *Multivariate Data Analysis: Global Edition*, 7th ed. Upper Saddle River, N.J: Pearson Education, 2010.

[84] A. P. Field, *Discovering statistics using IBM SPSS statistics*, 4th ed. SAGE Publications, 2013.

[85] Z. Zhang, "Variable selection with stepwise and best subset approaches," *Ann. Transl. Med.*, vol. 4, no. 7, 2016, doi: 10.21037/atm.2016.03.35.

[86] J. H. McDonald, "Handbook of Biological Statistics (online version)," 2014. http://www.biostathandbook.com/.

[87] N. Hirschauer et al., "Pitfalls of significance testing and p-value variability-implications for statistical inference," 2017. doi: https://doi.org/10.1214/18-SS122.

[88] M. Rubin, "Do p values lose their meaning in exploratory analyses? It depends how you define the familywise error rate," *Rev. Gen. Psychol.*, vol. 21, no. 3, 2017, doi: 10.1037/gpr0000123.

[89] E. D. Kilbourne, C. Smith, I. Brett, B. A. Pokorny, B. Johansson, and N. Cox, "The total influenza vaccine failure of 1947 revisited: Major intrasubtypic antigenic change can explain failure of vaccine in a post-World War II epidemic," *Proc. Natl. Acad. Sci. U. S. A.*, vol. 99, no. 16, 2002, doi: 10.1073/pnas.162366899.

[90] Y. Liu *et al.*, "Genetic variants in IL1A and IL1B contribute to the susceptibility to 2009 pandemic H1N1 influenza A virus," *BMC Immunol.*, vol. 14, no. 1, 2013, doi: 10.1186/1471-2172-14-37.

[91] N. Lee *et al.*, "Single-nucleotide polymorphisms of IFITM3, TLR3, CD55 , and TLR4 and risk for severe outcomes in patients with influenza A (H7N9) and (H1N1) pdm09 in China: a multicentre cohort study," *Lancet*, vol. 390, Dec. 2017, doi: 10.1016/S0140-6736(17)33139-2.

[92] C. M. Bui, A. A. Chughtai, D. C. Adam, and C. R. MacIntyre, "An overview of the epidemiology and emergence of influenza A infection in humans over time," *Archives of Public Health*, vol. 75, no. 1. BioMed Central Ltd., 2017, doi: 10.1186/s13690-017-0182-z.

[93] S. J. Olsen *et al.*, "Family clustering of avian influenza A (H5N1)," *Emerging Infectious Diseases*, vol. 11, no. 11. Centers for Disease Control and Prevention (CDC), 2005, doi: 10.3201/eid1111.050646.

[94] L. Yi *et al.*, "Family clusters of Avian influenza A H7N9 virus infection in Guangdong province, China," *J. Clin. Microbiol.*, vol. 53, no. 1, 2015, doi: 10.1128/JCM.02322-14.

[95] W. Friedberg and K. Copeland, "Ionizing Radiation in Earth's Atmosphere and in Space Near Earth Federal Aviation Administration," Oklahoma City, DOT/FAA/AM-11/9, 2011. [Online]. Available: https://www.faa.gov/data_research/research/med_humanfacs/oamtechreports/2010s/media/201109.pdf.

[96] G. Gruel *et al.*, "Broad modulation of gene expression in CD4+ lymphocyte subpopulations in

response to low doses of ionizing radiation," *Radiat. Res.*, vol. 170, no. 3, 2008, doi: 10.1667/RR1147.1.

[97] D. Vokurková et al., "CD8 + Natural Killer Cells Have a Potential of a Sensitive and Reliable Biodosimetric Marker in vitro," *Physiol. Res.*, vol. 55, 2006.

[98] S. M. Candéias *et al.*, "Low-dose radiation accelerates aging of the T-cell receptor repertoire in CBA/Ca mice," *Cell. Mol. Life Sci.*, vol. 74, no. 23, 2017, doi: 10.1007/s00018-017-2581-2.

[99] E. N. Bogdándi *et al.*, "Effects of low-dose radiation on the immune system of mice after total-body irradiation," *Radiat. Res.*, vol. 174, no. 4, 2010, doi: 10.1667/RR2160.1.

[100] F. M. Di Maggio *et al.*, "Portrait of inflammatory response to ionizing radiation treatment," *Journal of Inflammation (United Kingdom)*, vol. 12, no. 1. BioMed Central Ltd., Feb. 2015, doi: 10.1186/s12950-015-0058-3.

[101] R. I. F. Trindade *et al.*, "Speleothem record of geomagnetic South Atlantic Anomaly recurrence," *Proc. Natl. Acad. Sci. U. S. A.*, vol. 115, no. 52, 2018, doi: 10.1073/pnas.1809197115.

[102] R. G. Woolthuis, C. H. Van Dorp, C. Keşmir, R. J. De Boer, and M. Van Boven, "Long-term adaptation of the influenza A virus by escaping cytotoxic T-cell recognition," *Sci. Rep.*, vol. 6, 2016, doi: 10.1038/srep33334.

[103] M. D. Pauly, M. C. Procario, and A. S. Lauring, "A novel twelve class fluctuation test reveals higher than expected mutation rates for influenza A viruses," *Elife*, vol. 6, 2017, doi: 10.7554/eLife.26437.

[104] R. Chen and E. C. Holmes, "Avian influenza virus exhibits rapid evolutionary dynamics," *Mol. Biol. Evol.*, vol. 23, no. 12, Dec. 2006, doi: 10.1093/molbev/msl102.

[105] R. H. Alford, J. A. Kasel, J. R. Lehrich, and V. Knight, "Human responses to experimental infection with influenza a/equi 2 virus," *Am. J. Epidemiol.*, vol. 86, no. 1, 1967, doi: 10.1093/oxfordjournals.aje.a120723.

[106] J. A. Kasel and R. B. Couch, "Experimental Infection in Man and Horses with Influenza A Viruses," Bulletin of the World Health Organization, 1969. [Online]. Available: https://apps.who.int/iris/bitstream/handle/10665/262509/PMC2427734.pdf.

[107] T. Xie, B. D. Anderson, U. Daramragchaa, M. Chuluunbaatar, and G. C. Gray, "A review of evidence that equine influenza viruses are zoonotic," *Pathogens*, vol. 5, no. 3. MDPI AG, 2016, doi: 10.3390/pathogens5030050.

[108] E. S. Soilemetzidou *et al.*, "Bearing the brunt: Mongolian khulan (Equus hemionus hemionus) are exposed to multiple influenza A strains," *Vet. Microbiol.*, vol. 242, 2020, doi: 10.1016/j.vetmic.2020.108605.

[109] H. Zhu *et al.*, "Absence of adaptive evolution is the main barrier against influenza emergence in horses in Asia despite frequent virus interspecies transmission from wild birds," *PLoS Pathog.*, vol. 15, no. 2, Feb. 2019, doi: 10.1371/journal.ppat.1007531.

[110] U. Joseph, Y. C. F. Su, D. Vijaykrishna, and G. J. D. Smith, "The ecology and adaptive evolution of influenza A interspecies transmission," *Influenza and other Respiratory Viruses*, vol. 11, no. 1. Blackwell Publishing Ltd, 2017, doi: 10.1111/irv.12412.

[111] T. Alerstam *et al.*, "A polar system of intercontinental bird migration," *Proc. R. Soc. B Biol. Sci.*, vol. 274, no. 1625, 2007, doi: 10.1098/rspb.2007.0633.

[112] B. Bruderer, D. Peter, and F. Korner-Nievergelt, "Vertical distribution of bird migration between the Baltic Sea and the Sahara," *Journal of Ornithology*, vol. 159, no. 2. Springer Verlag, 2018, doi: 10.1007/s10336-017-1506-z.

[113] M. Martinez-Bakker and B. Helm, "The influence of biological rhythms on host-parasite interactions," *Trends in Ecology and Evolution*, vol. 30, no. 6. Elsevier Ltd, 2015, doi: 10.1016/j.tree.2015.03.012.

[114] A. Hegemann et al., “Immune function in a free-living bird varies over the annual cycle, but seasonal patterns differ between years,” *Oecologia*, vol. 170, no. 3, 2012, doi: 10.1007/s00442-012-2339-3.

[115] M. A. Versteegh et al., “Genetic and phenotypically flexible components of seasonal variation in immune function,” *J. Exp. Biol.*, vol. 217, no. 9, 2014, doi: 10.1242/jeb.097105.

[116] D. Ottaviani *et al.*, “The cold European winter of 2005-2006 assisted the spread and persistence of H5N1 influenza virus in wild birds,” *Ecohealth*, vol. 7, no. 2, 2010, doi: 10.1007/s10393-010-0316-z.

[117] C. M. Liu et al., “Temperature drops and the onset of severe avian influenza A H5N1 virus outbreaks,” *PLoS One*, vol. 2, no. 2, 2007, doi: 10.1371/journal.pone.0000191.

[118] H. Q. P. Crick *et al.*, “Avian Influenza incursion analysis (through wild birds) | BTO - British Trust for Ornithology,” Thetford, Norfolk, 2006. [Online]. Available: https://www.bto.org/sites/default/files/shared_documents/publications/research-reports/2006/rr448.pdf.

[119] N.-A. Mörner *et al.*, “General conclusions regarding the planetary–solar–terrestrial interaction,” *Pattern Recognit. Phys.*, vol. 1, no. 1, 2013, doi: 10.5194/prp-1-205-2013 (access the related publications http://www.pattern-recogn-phys.net/1/issue1.html, http://www.pattern-recogn-phys.net/2/issue1.html).

[120] N.-A. Mörner, “Planetary beat and solar–terrestrial responses,” *Pattern Recognit. Phys.*, vol. 1, no. 1, 2013, doi: 10.5194/prp-1-107-2013.

[121] N. Scafetta, “Empirical evidence for a celestial origin of the climate oscillations and its implications,” *J. Atmos. Solar-Terrestrial Phys.*, vol. 72, no. 13, 2010, doi: 10.1016/j.jastp.2010.04.015.

[122] J.-E. Solheim, “Signals from the planets, via the Sun to the Earth,” *Pattern Recognit. Phys.*, vol. 1, no. 1, 2013, doi: 10.5194/prp-1-177-2013.

[123] N. A. Mörner, “Solar Minima, Earth’s rotation and Little Ice Ages in the past and in the future. The North Atlantic-European case,” *Glob. Planet. Change*, vol. 72, no. 4, 2010, doi: 10.1016/j.gloplacha.2010.01.004.

[124] “Scientific publications (n = 190): solar activity controlled climate change, glacial cycle stage, the Little Ice Age, volcanism, grand solar minimum risks.” https://grandsolarminimum.com/scientific-publication-hyperlinks.

[125] C. Martín-Puertas, I. LastNameDorado-Liñán1, A. Brauer, E. Zorita, B. L. Valero-Garcés, and E. Gutierrez, “Hydrological evidence for a North Atlantic oscillation during the Little Ice Age outside its range observed since 1850,” *Clim. Past Discuss.*, vol. 7, no. 6, 2011, doi: 10.5194/cpd-7-4149-2011.

[126] S. B. Wirth, L. Glur, A. Gilli, and F. S. Anselmetti, “Holocene flood frequency across the Central Alps - solar forcing and evidence for variations in North Atlantic atmospheric circulation,” *Quat. Sci. Rev.*, vol. 80, 2013, doi: 10.1016/j.quascirev.2013.09.002.

[127] B. Wilhelm *et al.*, “1400years of extreme precipitation patterns over the Mediterranean French Alps and possible forcing mechanisms,” *Quat. Res.*, vol. 78, no. 1, 2012, doi: 10.1016/j.yqres.2012.03.003.

[128] L. Tan, Y. Cai, L. Yi, Z. An, and L. Ai, “Precipitation variations of Longxi, northeast margin of Tibetan Plateau since AD 960 and their relationship with solar activity,” *Clim. Past*, vol. 4, no. 1, 2008, doi: 10.5194/cp-4-19-2008.

[129] W. Deng *et al.*, “A comparison of the climates of the Medieval Climate Anomaly, Little Ice Age, and Current Warm Period reconstructed using coral records from the northern South China Sea,” *J. Geophys. Res. Ocean.*, vol. 122, no. 1, 2017, doi: 10.1002/2016JC012458.

1173 [130] J. J. Yin *et al.*, “Variation in the Asian monsoon intensity and dry-wet conditions since the little
1174 ice age in central china revealed by an aragonite stalagmite,” *Clim. Past*, vol. 10, no. 5, 2014, doi:
1175 10.5194/cp-10-1803-2014.
1176 [131] H. Xu *et al.*, “Late Holocene Indian summer monsoon variations recorded at Lake Erhai,
1177 Southwestern China,” *Quat. Res.*, vol. 83, no. 2, 2015, doi: 10.1016/j.yqres.2014.12.004.
1178 [132] Z. Yu and E. Ito, “Possible solar forcing of century-scale drought frequency in the northern Great
1179 Plains,” *Geology*, vol. 27, no. 3, 1999, doi: doi.org/10.1130/0091-
1180 7613(1999)027<0263:PSFOCS>2.3.CO;2.
1181 [133] J. E. Nichols and Y. Huang, “Hydroclimate of the northeastern United States is highly sensitive to
1182 solar forcing,” *Geophys. Res. Lett.*, vol. 39, no. 4, 2012, doi: 10.1029/2011GL050720.
1183 [134] G. Bond *et al.*, “Persistent solar influence on north atlantic climate during the Holocene,” *Science
1184 (80-. ).*, vol. 294, no. 5549, 2001, doi: 10.1126/science.1065680.
1185 [135] J. Slawinska and A. Robock, “Impact of volcanic eruptions on decadal to centennial fluctuations
1186 of Arctic sea ice extent during the Last Millennium and on initiation of the Little Ice Age,” *J.
1187 Clim.*, vol. 31, no. 6, 2018, doi: 10.1175/JCLI-D-16-0498.1.
1188 [136] F. Lehner, A. Born, C. C. Raible, and T. F. Stocker, “Amplified inception of European little Ice
1189 Age by sea ice-ocean-atmosphere feedbacks,” *J. Clim.*, vol. 26, no. 19, 2013, doi: 10.1175/JCLI-
1190 D-12-00690.1.
1191 [137] Y. Zhong *et al.*, “Centennial-scale climate change from decadally-paced explosive volcanism: A
1192 coupled sea ice-ocean mechanism,” *Clim. Dyn.*, vol. 37, no. 11–12, 2011, doi: 10.1007/s00382-
1193 010-0967-z.
1194 [138] S. K. Solanki, I. G. Usoskin, B. Kromer, M. Schüssler, and J. Beer, “Unusual activity of the Sun
1195 during recent decades compared to the previous 11,000 years,” *Nature*, 2004.
1196 https://doi.org/10.1038/nature02995. [data: https://www.ncdc.noaa.gov/paleo-search/study/5780].
1197 [139] N. K. Larsen *et al.*, “The response of the southern Greenland ice sheet to the Holocene thermal
1198 maximum,” *Geology*, vol. 43, no. 4, 2015, doi: 10.1130/G36476.1.
1199 [140] J. P. Briner *et al.*, “Holocene climate change in Arctic Canada and Greenland,” *Quaternary
1200 Science Reviews*, vol. 147. Elsevier Ltd, 2016, doi: 10.1016/j.quascirev.2016.02.010.
1201 [141] Ó. Ingólfsson *et al.*, “Antarctic glacial history since the Last Glacial Maximum: An overview of
1202 the record on land,” *Antarct. Sci.*, vol. 10, no. 3, 1998, doi: 10.1017/s095410209800039x.
1203 [142] H. Wanner, O. Solomina, M. Grosjean, S. P. Ritz, and M. Jetel, “Structure and origin of Holocene
1204 cold events,” *Quat. Sci. Rev.*, vol. 30, no. 21–22, 2011, doi: 10.1016/j.quascirev.2011.07.010.
1205 [143] D. S. Kaufman *et al.*, “Holocene thermal maximum in the western Arctic (0-180°W),” *Quat. Sci.
1206 Rev.*, vol. 23, no. 5–6, 2004, doi: 10.1016/j.quascirev.2003.09.007.
1207 [144] I. Borzenkova et al., “Climate Change During the Holocene (Past 12,000 Years),” in *The BACC II
1208 Author Team, Second Assessment of Climate Change for the Baltic Sea Basin. Regional Climate
1209 Studies*, Springer, Cham., 2015.
1210 [145] US Environmental Protection Agency, “Climate Change Indicators: Climate Forcing.”
1211 https://www.epa.gov/climate-indicators/climate-change-indicators-climate-forcing#ref1 (accessed
1212 Jun. 29, 2021).
1213 [146] L. Polyak *et al.*, “History of sea ice in the Arctic,” *Quat. Sci. Rev.*, vol. 29, no. 15–16, 2010, doi:
1214 10.1016/j.quascirev.2010.02.010.
1215 [147] N. L. Balascio, W. J. D’Andrea, and R. S. Bradley, “Glacier response to North Atlantic climate
1216 variability during the Holocene,” *Clim. Past*, vol. 11, no. 12, 2015, doi: 10.5194/cp-11-1587-2015.
1217 [148] M. Frezzotti, C. Scarchilli, S. Becagli, M. Proposito, and S. Urbini, “A synthesis of the Antarctic
1218 surface mass balance during the last 800 yr,” *Cryosphere*, vol. 7, no. 1, 2013, doi: 10.5194/tc-7-

303-2013.

[149] Ó. Ingólfsson, C. Hjort, and O. Humlum, “Glacial and Climate History of the Antarctic Peninsula since the Last Glacial Maximum,” *Arctic, Antarct. Alp. Res.*, vol. 35, no. 2, 2003, doi: 10.1657/1523-0430(2003)035[0175:GACHOT]2.0.CO;2.

[150] F. Taylor, J. Whitehead, and E. Domack, “Holocene paleoclimate change in the Antarctic Peninsula: Evidence from the diatom, sedimentary and geochemical record,” *Mar. Micropaleontol.*, vol. 41, no. 1–2, 2001, doi: 10.1016/S0377-8398(00)00049-9.

[151] “What will happen during a new Maunder Minimum?,” *Guest blogs by 5 five solar scientists expert in climate change: Mike Lockwood, Nicola Scafetta, Jan-Erik Solheim, José Vaquero and Ilya Usoskin.*, 2014. https://mwenb.nl/what-will-happen-during-a-new-maunder-minimum/ (accessed Jun. 29, 2021).

[152] H. Abdussamatov, “Current long-term negative average annual energy balance of the earth leads to the new little Ice Age,” *Therm. Sci.*, vol. 19, 2015, doi: 10.2298/TSCI140902018A.

[153] T. Landscheidt, “New Little Ice Age instead of global warming?,” *Energy Environ.*, vol. 14, no. 2–3, 2003, doi: 10.1260/095830503765184646.

[154] N. Scafetta, “Multi-scale harmonic model for solar and climate cyclical variation throughout the Holocene based on Jupiter-Saturn tidal frequencies plus the 11-year solar dynamo cycle,” *J. Atmos. Solar-Terrestrial Phys.*, vol. 80, 2012, doi: 10.1016/j.jastp.2012.02.016.

[155] R. J. Salvador, “A mathematical model of the sunspot cycle for the past 1000 yr,” *Pattern Recognit. Phys.*, vol. 1, no. 1, 2013, doi: 10.5194/prp-1-117-2013.

[156] J. L. Goodman, “Investing in Immunity: Prepandemic Immunization to Combat Future Influenza Pandemics,” *Clin. Infect. Dis.*, vol. 62, no. 4, 2015, doi: 10.1093/cid/civ957.

[157] G. Milne, J. Kelso, and H. Kelly, “Strategies for mitigating an influenza pandemic with pre-pandemic H5N1 vaccines,” *J. R. Soc. Interface*, vol. 7, no. 45, 2010, doi: 10.1098/rsif.2009.0312.

[158] R. Rappuoli and P. R. Dormitzer, “Influenza: Options to improve pandemic preparation,” *Science*, vol. 336, no. 6088. American Association for the Advancement of Science, 2012, doi: 10.1126/science.1221466.

[159] K. Stöhr, “Vaccinate before the next pandemic?,” *Nature*, May 2010, doi: 10.1038/465161a.

[160] G. Galli *et al.*, “Fast rise of broadly cross-reactive antibodies after boosting long-lived human memory B cells primed by an MF59 adjuvanted prepandemic vaccine,” *Proc. Natl. Acad. Sci.*, vol. 106, no. 19, 2009, doi: 10.1073/pnas.0903181106.

[161] P. Gillard *et al.*, “Long-term booster schedules with AS03A-adjuvanted heterologous H5N1 vaccines induces rapid and broad immune responses in Asian adults,” *BMC Infect. Dis.*, vol. 14, no. 1, 2014, doi: 10.1186/1471-2334-14-142.

[162] D. Stadlbauer *et al.*, “Vaccination with a Recombinant H7 Hemagglutinin-Based Influenza Virus Vaccine Induces Broadly Reactive Antibodies in Humans,” *mSphere*, vol. 2, no. 6, Dec. 2017, doi: 10.1128/mSphere.00502-17.